Density dependence in the two-nucleon effective interaction at 135 MeV

J. J. Kelly
Department of Physics and Astronomy, University of Maryland, College Park, Maryland 20742

W. Bertozzi, T. N. Buti,[a] J. M. Finn,[b] F. W. Hersman,[c] C. Hyde-Wright,[d] M. V. Hynes,[e] M. A. Kovash,[f] B. Murdock,[g] B. E. Norum,[h] B. Pugh,[f] and F. N. Rad[i]
Department of Physics and Laboratory for Nuclear Science, Massachusetts Institute of Technology, Cambridge, Massachusetts 02139

A. D. Bacher, G. T. Emery,[j] C. C. Foster, W. P. Jones, and D. W. Miller
Department of Physics, Indiana University, Bloomington, Indiana 47401

B. L. Berman
Department of Physics, George Washington University, Washington, D.C. 20052

W. G. Love
Department of Physics and Astronomy, University of Georgia, Athens, Georgia 30602

J. A. Carr
Supercomputer Computations Research Institute and Department of Physics and Astronomy, Florida State University, Tallahassee, Florida 32306

F. Petrovich
Department of Physics, Florida State University, Tallahassee, Florida 32306
(Received 31 October 1988)

Differential cross sections and analyzing powers for scattering of 135-MeV protons by ^{16}O have been measured for all narrow states below 12.1 MeV of excitation up to a momentum transfer of 3.2 fm^{-1}. Calculations that employ accurate transition densities fitted to electroexcitation data are used to study medium modifications to the two-nucleon effective interaction with little residual uncertainty from nuclear structure. Definitive evidence for strong density dependence in the isoscalar spin-independent central component of the two-nucleon effective interaction has been found. The differential cross sections show that as the density increases, the strength of the central interaction is suppressed at low momentum transfer and enhanced at high momentum transfer. The analyzing powers exhibit strong negative excursions near 2.5 fm^{-1}, which support enhanced repulsion at high density. The data are well described by the local-density approximation, which employs the nuclear-matter effective interaction appropriate to the density in the vicinity of the interacting nucleons. We find that the qualitative results are insensitive to ambiguities in the local-density prescription, the local-exchange approximation, and the choice of distorted waves. However, effective interactions based upon the Paris, Bonn, and Hamada-Johnston potentials do give substantially different results. Of these, the Paris-Hamburg effective interaction provides the best description of normal-parity isoscalar transitions. The analysis also supports a rearrangement contribution to the effective interaction for inelastic scattering.

I. INTRODUCTION

The effective interaction between a projectile nucleon and a target nucleon can be substantially modified by the presence of a nuclear medium.[1] In particular, Pauli blocking is known to produce strong density dependence in the effective interaction for projectile energies below 200 MeV.[2–5] Below 100 MeV, the effective interaction is similar to the G-matrix between nucleons bound in nuclear matter.[6–9] The G-matrix theory of the optical potential has been developed in considerable detail by Hüfner and Mahaux.[10] Based upon this approach, several groups have constructed density-dependent effective interactions for nuclear matter using a variety of free potentials and approximation strategies.[11–16] These interactions may be applied to scattering using the local density approximation (LDA), in which it is assumed that the effective interaction between an energetic projectile and a nucleon bound in a finite system is essentially the same as that appropriate to infinite nuclear matter with the local density.[17,18] Our objective is to compare these

interactions using intermediate energy scattering data for which the reaction mechanism is expected to be simplest;[19,20] other groups have made similar comparisons at lower energies where additional complications are encountered.[21–23] We use transition densities measured with electron scattering to minimize ambiguities due to nuclear structure.[24]

The best understood probe of nuclear structure is the electron, whose perturbative one-step electromagnetic interaction with the nucleus can be readily and precisely interpreted in terms of the radial distributions of charge, current, and magnetization that characterize the nuclear states involved.[25,26] The simplest class of nuclear transitions for which electron-scattering measurements most completely determine the nuclear structure required to interpret nucleon scattering consists of those normal-parity isoscalar transitions in an $N=Z$ nucleus for which the transverse form factor nearly vanishes over a substantial range of momentum transfer.[27,28] For these transitions, the only transition densities involved in either electron or proton scattering are the proton and neutron matter densities. Although it is possible for the convection and spin contributions to the transverse form factor to cancel over a limited range of momentum transfer, the observation that the transverse form factor nearly vanishes over a substantial range of momentum transfer severely limits the intensity of each contribution. Furthermore, charge symmetry ensures that, to a high degree of accuracy, the proton and neutron transition densities for isoscalar excitations of a self-conjugate nucleus are equal. Therefore, electroexcitation measurements of the transition charge density suffice to completely specify the nuclear structure required to study this class of transitions by nucleon scattering.

In order to test the effective interaction, it is necessary to obtain data for a wide variety of states for which the nuclear structure is known. An excellent laboratory for this study is provided by ^{16}O, for which states of many multipolarities can be resolved with only modest resolution. States of low multipolarity, such as 0^+ and 1^-, peak in the high-density nuclear interior where the medium modifications are largest. States of higher multipolarity, such as 3^- and 4^+, peak in the low-density nuclear surface and are sensitive to the effective interaction at low density.

We have measured cross sections and analyzing powers for the scattering of 135 MeV protons by ^{16}O over the range of momentum transfer $q=0.3$–3.2 fm^{-1}, observing three 0^+ states (0_1^+ at 0.0, 0_2^+ at 6.049, and 0_3^+ at 12.053 MeV), one 1^- state at 7.117 MeV, three 2^+ states (2_1^+ at 6.917, 2_2^+ at 9.847, and 2_3^+ at 11.521 MeV), one 3^- state at 6.130 MeV, and two 4^+ states (4_1^+ at 10.353 and 4_2^+ at 11.09 MeV). The elastic scattering data reach 3.5 fm^{-1}. Electroexcitation measurements spanning momentum transfers between about 0.4 and 2.7 fm^{-1} were reported in Ref. 24 for all of these states. The accurate transition densities fitted to these data provide the structure information required to interpret the present data for proton scattering with little residual ambiguity.

Early results from this experiment provided the first demonstration that the deficiencies of the impulse approximation (IA) for proton energies between 100 and 200 MeV may be interpreted as evidence for strong density-dependence in the isoscalar spin-independent central component of the effective interaction.[19] Similar results were also shown for ^{12}C and ^{40}Ca. That analysis employed an effective interaction (BRG) constructed by Brieva, Rook, and von Geramb[12,29] using the Hamada-Johnston potential.[30] The strong density dependence of the BRG interaction provided a good description of inelastic cross section and analyzing power data but was too severe for elastic scattering.

Subsequently, von Geramb and his Hamburg associates[13,14] produced a new effective interaction (PH) based upon the Paris potential.[31] In contrast to the BRG interaction, the PH interaction was found to provide a good description of elastic scattering data for ^{12}C, ^{208}Pb, and several other nuclei for energies between 100 and 400 MeV.[14,32,33] Similar results for ^{16}O were reported in Ref. 34, for ^{12}C in Ref. 35, for ^{28}Si in Ref. 36, and for ^{24}Mg and ^{28}Si in Ref. 37. However, using a more complete set of data, we found that inelastic data prefer stronger medium modifications intermediate between those of the PH and BRG interactions.[38] In contrast with Refs. 34–37, which adjust model wave functions to achieve qualitative agreement with (e,e') data, our use of measured transition densities permits quantitative comparisons to be made.

Part of the apparent discrepancy between elastic and inelastic scattering was shown by Cheon *et al.*[39,40] to be attributable to neglect in these early calculations of an important rearrangement contribution that essentially doubles the density dependence of the interaction responsible for inelastic scattering. When this contribution is included, the PH interaction also provides a good description of normal-parity excitations for which the transition density is interior in nature.[41] Surface transitions still seem to require stronger density dependence. Several analyses which fit an empirical effective interaction to data were reported in Refs. 41–43.

Finally, another interaction based upon the Bonn potential[44] was constructed by Nakayama and Love (NL).[15] At 135 MeV, the density dependence of the real part of t_{00}^C is weaker and that of the imaginary part is stronger in the NL interaction than in the PH interaction. Although all three effective interactions are similar at low density, important differences are obtained for any transition with significant interior strength. Therefore, we present a systematic comparison of these three effective interactions with data for the excitation of many states of ^{16}O by 135 MeV protons. The usefulness of this study is enhanced by the availability of high-quality data for interior transitions in addition to the more easily accessible collective states.

The experimental procedure and data analysis are presented in Sec. II. The reaction model is described in Sec. III. Elastic scattering results are presented in Sec. IV and inelastic scattering in Sec. V. These results are discussed further in Sec. VI, wherein the approximations made in constructing the effective interactions are reviewed critically. Our conclusions are summarized in Sec. VII.

II. EXPERIMENT

A. Experimental procedure

The Indiana University cyclotron provided up to 200 nA of 135 MeV protons on target. Both polarized and unpolarized sources were used. The beam was dispersed on target with a $\delta p/p = \pm 0.1\%$ spread in a 3×3 mm spot. The scattered protons were analyzed by the dispersion matched QDDM magnetic spectrometer. The detector array, placed approximately in the focal plane position, consisted of a position-sensitive helical wire chamber and two plastic scintillators. The plastic scintillators, 7 and 12 mm thick, provided $\Delta E1$ and $\Delta E2$ for particle identification. The position in the focal plane was measured by the time difference between induced signals reaching either end of the helical cathode wire. A fast triple coincidence between the chamber anode signal and the discriminated outputs from the scintillators gated the time-to-amplitude converter (TAC) and the linear outputs from the scintillators, which were then processed by an analog-to-digital converter (ADC) system.

Dead time was monitored by passing pulser signals, triggered at a rate proportional to the beam current, through all detectors and processing these signals as ordinary events. The accuracy of the dead-time correction was verified by observing that cross sections measured with 30% dead-time losses reproduced, within statistics, those measured with losses of a few percent. Dead-time losses were generally kept below 10%.

The spectrometer acceptance was defined by jaws at the spectrometer entrance and set with calibrated precision micrometer screws. Acceptances in the range of 12–18 mrad (full opening) in the momentum direction and 24–60 mrad in the transverse direction were used. The relative solid angles were verified by repeating a measurement after a solid-angle setting was changed.

The energy resolution obtained with the smallest solid-angle setting and a thin target was about 45 keV full width at half maximum (FWHM). The energy resolution deteriorates rapidly as the acceptance is increased, becoming about 120 keV for an acceptance of 18 by 60 mrad.

The total beam charge was measured by Faraday cup beam catchers downstream from the target. For scattering angles larger than 24° the beam catcher may be placed in the beam line external to the scattering chamber. For scattering angles less than 24° the spectrometer intercepts the downstream beam line, making it necessary to place the beam catcher internal to the scattering chamber, which greatly increases the background. Finally, a split internal cup, separately integrating the charge collected in its left and right halves, was also used. The external cup is believed to be accurate to about 1% but the internal cups are subject to several energy-dependent normalization difficulties.[45] Measurements repeated with the various cups showed that the normalization of the internal cups differed from that of the external cup by about 3%. This correction has been applied to the data taken with the internal cup.

The scattering-angle offset was determined by two methods. First, elastic cross sections were measured at several angles on either side of the beam line. Second, the differential recoil of several isotopes were fitted at many angles. Both methods gave offsets of 0.05°–0.12°.

The focal-plane relative efficiency was checked by varying the spectrometer magnetic field and thereby moving the elastic peaks across the focal plane. The relative efficiency was found to be constant within the statistics of the measurement ($\sim 1\%$).

The targets were beryllium oxide (BeO) wafers. The targets manufactured from naturally occurring oxygen ranged in thickness from 20 to 239 mg/cm^2. The targets were usually oriented in transmission geometry with the target normal bisecting the scattering angle. Several mixed-isotope targets, enriched in ^{17}O and ^{18}O, were also used. The elastic peaks are separated by differential recoil. The isotopic abundances were determined by using the ratio of the oxygen yields to the beryllium yields for several different targets. The manufacture and isotopic analysis of these targets is described in Ref. 46. Cross sections measured with different targets were found to reproduce within ± 3–5 %.

For each of six strong peaks, approximately ten cross-section measurements were repeated in the separate runs that comprise the present experiment. For each of these peaks the average ratio between runs was unity, with a scatter of 2–3 % and with no systematic dependence on scattering angle. However, for the earliest run the normalization appears to differ from that of the later runs by about 5%, although no data from that run is reported here. Combining this information with the uncertainty in the target thicknesses, we estimate that the overall normalization uncertainty is about $\pm 5\%$.

For all cross sections entering in the above normalization comparison the statistical precision was better than 1%. The larger scatter of 2–3 % is consistent with the normalization fluctuation observed internal to each run. It has been found that the ratios of cross sections measured in the same exposure agree within statistics, but that the normalization between repeated measurements tends to fluctuate by $\pm 2\%$. This fluctuation has been observed in many circumstances. The source of this fluctuation has not been definitely identified, but is probably related to beam integration. Therefore, a $\pm 2\%$ uncertainty has been added in quadrature to the statistical and fitting uncertainties for the cross-section measurements.

For the analyzing-power measurements, the polarized source was operated in fast spin-flip mode, automatically reversing the beam polarization about once per minute. This procedure minimizes false asymmetries that arise in single-arm measurements due to normalization and beam-position drifts. We assume that there is no correlation between beam orientation and integration. Therefore, the normalization fluctuation should be averaged out of the analyzing power by the fast spin-flip and is not included in the estimation of analyzing-power uncertainties.

As there was no continuous on-line polarimeter, the beam polarization was measured every few hours using a ^{4}He gas cell that can be lowered into the beam line between the injector and main-stage cyclotrons. Surface barrier detectors placed symmetrically on either side of

the beam line at scattering angles of $\pm 122°$ were used to measure the left-right asymmetry for both beam orientations. The intrinsic detector asymmetry, due to differences in detector geometry or efficiency, was measured with an unpolarized beam obtained from the outgassing of the walls of the source when the atomic beam valve was closed. This asymmetry differed from unity by about 3%. The proton energy between the cyclotrons was 11.19 MeV. Over a broad range of similar energies, the ^{4}He analyzing power is known to be essentially unity at the chosen scattering angle.[47]

The beam polarization for each orientation was measured to a statistical precision of 0.3%. The polarization for spin-up was generally about 73% and the spin-down about 70%. The beam polarization was measured approximately once every four hours and was found to drift by no more than about 1% between measurements.

This technique measures the beam polarization between the two cyclotrons. That the depolarization during main-stage acceleration is negligible has been verified by Schwandt *et al.*[48] by remeasuring ^{12}C elastic analyzing powers at several energies. These measurements reproduced the results of earlier double-scattering experiments. The measurement in the present and other experiments of elastic analyzing powers larger than 0.97 places an upper limit on depolarization during main-stage acceleration of 3%.

B. Data Analysis

The scattered proton spectra were fitted with a line-shape fitting code, PPFIT,[49] that employs an empirical line shape. The origin of this shape lies in the spectrometer aberrations, target mass and thickness, and beam tuning. The shape may be described as an asymmetric "hyper-Gaussian" in the central region plus exponential tails and is given by

$$y(x)=\begin{cases} f_L H e^{-\lambda_L (p-m_L-x)}, & x \le p-m_L \\ H e^{-|x-p|^{\gamma}/2\sigma^2(1-\alpha)^2}, & p-m_L \le x \le p \\ H e^{-|x-p|^{\gamma}/2\sigma^2(1+\alpha)^2}, & p \le x \le p+m_R \\ f_R H e^{-\lambda_R (x-p-m_R)}, & p+m_R \le x \end{cases} \quad (1)$$

where the nine parameters consist of the height H, position p, width σ, asymmetry α, exponent γ, left and right match points m_L and m_R, and left and right slopes λ_L and λ_R. The factors of f_L and f_R are chosen to ensure continuity. In a small region surrounding the match points, smoothing is achieved by replacing the function with

$$y(x)=e^{a+bx+cx^2+dx^3}, \quad (2)$$

where the parameters are chosen to ensure continuity and smoothness. A cubic background is included.

Sample spectra are shown in Fig. 1 for the elastic region and Fig. 2 for 5.5–12.5 MeV of excitation energy in ^{16}O. The abrupt rise in the background in Fig. 1 is due to the $^9\text{Be} \rightarrow {}^8\text{Be}+n$ decay threshold. The $\frac{1}{2}^+$ state of ^{9}Be is only 15 keV above threshold and hence its line shape is quite asymmetric. A broad Lorentzian peak about 6.5 MeV above the ^{9}Be ground state dominates the continuum in Fig. 2. The narrow peaks exhibit asymmetric central shapes and prominent tails, particularly on the side with low projectile energy. Fitting with simple Gaussian line shapes, without the tails or the sophisticated central shape of Eq. (1), often misses more than 10% of the area. These problems are particularly severe for small peaks on large backgrounds, but are eliminated for inelastic spectra such as Fig. 2 by employing the tails fitted to elastic spectra.

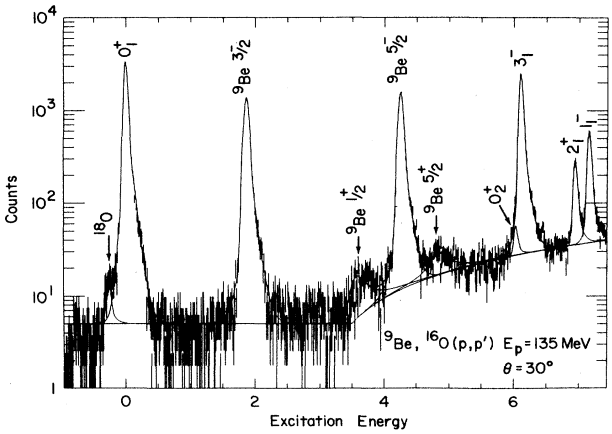

FIG. 1. Sample spectrum for scattering of 135 MeV protons through 30° by a BeO target. In addition to the total fit, separate contributions are shown for the background and for each peak.

The search code uses the routine CURFIT,[50] modified to employ a correct Poisson,[49,24] rather than Gaussian, goodness-of-fit criterion. As the Poisson distribution is strongly peaked at the correct area, the traditional Gaussian under fitting of low-statistics data is eliminated.

The code provides for considerable flexibility. Any or

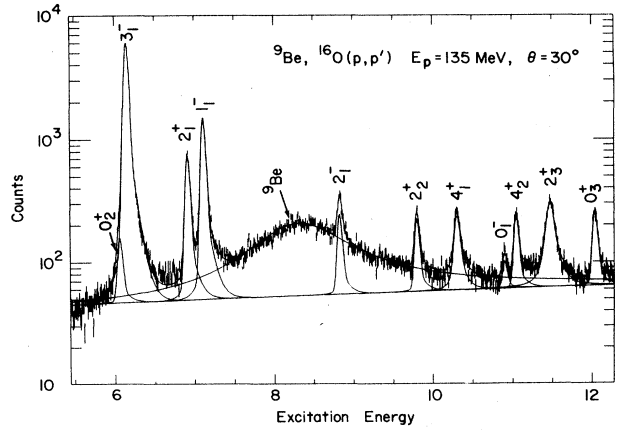

FIG. 2. Sample spectrum for the 5.5–12.5 MeV excitation region of ^{16}O obtained by scattering 135 MeV protons through 30° using a BeO target. Note that although the kinematic conditions are similar to those of Fig. 1, these two spectra were acquired independently with different spectrometer settings.

all of the parameters may be free to vary or may be fixed to input values. Parameters may be locked to the corresponding parameter in another peak. In the case of peak height, locking constrains the ratio of the peak heights to the ratio of their initial values. In the case of position, locking constrains the separation between peaks to their initial separation. For all other parameters, locking maintains numerical equality between locked parameters. All peaks sharing a locked parameter contribute to its determination.

This flexible search procedure often enables reliable extraction of unresolved peaks. When the levels of interest have negligible intrinsic width, unresolved peaks can be fitted by locking their shapes to that of some strong isolated peak and locking their separation to their known kinematic separation. Only the peak heights and a single overall cluster position are allowed to vary. That this procedure is reliable has been verified by several methods, including reproducibility, use of different target thicknesses, and use of different isotopic mixtures. The most stringent such test was the separation of the weak 0^+ state at 6.049 MeV from the much stronger 3^- state at 6.130 MeV. This cross section was reproducible from run to run and was independent of target thickness and energy resolution.

Data tables are available from PAPS.[51] In addition to the normal-parity states considered in this paper, these tables include data for the 0_1^- and 2_1^- states of ^{16}O and for the $(3/2)_1^-$ and $(5/2)_1^-$ states of ^{9}Be. Preliminary versions of these 0^- data have appeared in several recent publications.[52,53] The ^{9}Be data were presented in Ref. 54.

III. REACTION MODEL

In this section, we present a relatively complete description of the model and the approximations upon which our calculations are based. Although much of this material is fairly standard,[55] its inclusion will make it easier to compare interactions and to discuss sensitivity to approximations.

A. Local pseudopotential

A local pseudopotential with central, spin-orbit, and tensor components can be written in the form[56]

$$V=\sum_{ST} V_{ST}^{C}(r)P_S P_T+\sum_{T} V_T^{LS}(r)\mathbf{L}\cdot\mathbf{S}P_T + \sum_{T} V_T^{T}(r)S_{12}(\hat{\mathbf{r}})P_T \ , \tag{3}$$

where P_S and P_T are spin and isospin projection operators. Antisymmetrized matrix elements of the pseudopotential are required to reproduce the on-shell t-matrix

$$\tilde{t}_{NN}(\mathbf{k}_f,\mathbf{k}_i)=\langle \mathbf{k}_f|V(1-X)|\mathbf{k}_i\rangle \ , \tag{4}$$

where X is the exchange operator. Hence, the t-matrix assumes the form

$$\tilde{t}_{NN}(q,Q)=\sum_{ST}\tilde{t}_{ST}^{C}P_S P_T+i\sum_{T}\tilde{t}_T^{LS}(\boldsymbol{\sigma}_1+\boldsymbol{\sigma}_2)\cdot\hat{\mathbf{n}}P_T - \sum_{T}[\tilde{V}_T^{T}(q)S_{12}(\hat{\mathbf{q}}) -(-)^{1+T}\tilde{V}_T^{T}(Q)S_{12}(\hat{\mathbf{Q}})]P_T \ , \tag{5}$$

where $\mathbf{q}=\mathbf{k}_i-\mathbf{k}_f$, $\mathbf{Q}=\mathbf{k}_i+\mathbf{k}_f$, and $\hat{\mathbf{n}}=\hat{\mathbf{q}}\otimes\hat{\mathbf{Q}}$, and where

$$\tilde{t}_{ST}^{C}=\tilde{V}_{ST}^{C}(q)-(-)^{S+T}\tilde{V}_{ST}^{C}(Q) \ , \tag{6a}$$

$$\tilde{t}_T^{LS}=\tfrac{1}{4}qQ[\tilde{V}_T^{LS}(q)+(-)^{1+T}\tilde{V}_T^{LS}(Q)] \ . \tag{6b}$$

The Fourier transforms are defined as

$$\tilde{V}^{C}(q)=4\pi\int dr\, r^2 j_0(qr)V^{C}(r) \ , \tag{7a}$$

$$\tilde{V}^{LS}(q)=4\pi\int dr\, r^4\frac{j_1(qr)}{qr}V^{LS}(r) \ , \tag{7b}$$

$$\tilde{V}^{T}(q)=4\pi\int dr\, r^2 j_2(qr)V^{T}(r) \ . \tag{7c}$$

For later use, we will also find it convenient to introduce

$$\tilde{\tau}_T^{LS}(q,Q)=-\tfrac{1}{4}[\tilde{V}_T^{LS}(q)+(-)^{1+T}\tilde{V}_T^{LS}(Q)] \ . \tag{8}$$

The most transparent formulation of nucleon-nucleus scattering is based upon the local exchange approximation,[7] which has been shown to be an accurate approximation for most normal-parity transitions excited by protons with $E_p \gtrsim 100$ MeV.[57–59] Of the several variations available, the simplest is the zero-range exchange approximation (ZREA), for which

$$\tilde{t}_{NA}(q)=\eta\tilde{t}_{NN}(q,k_A) \ , \tag{9}$$

where η is a Jacobian of order unity[1,56] and k_A is the projectile wave number in the NA center of mass. Thus, exchange interactions are independent of momentum transfer and reduce to delta functions.

The effective interaction for normal-parity isoscalar transitions with negligible spin and current densities reduces to

$$\tilde{t}=\tilde{t}^{C}(q)+i\tilde{t}^{LS}(q)\boldsymbol{\sigma}\cdot\hat{\mathbf{n}} \ , \tag{10}$$

where $\boldsymbol{\sigma}$ describes the projectile spin. Exchange is included in the pseudopotential approximation and unnecessary labels are omitted. In plane wave impulse approximation (PWIA), the cross section and analyzing power for a normal-parity transition between target spins I_i and I_f reduce to

$$\frac{d\sigma}{d\Omega}=4\pi\frac{2I_f+1}{2I_i+1}\left[\frac{\mu}{2\pi}\right]^2[|\tilde{t}^{C}(q)|^2+|\tilde{t}^{LS}(q)|^2]|\tilde{\rho}_J(q)|^2 \ , \tag{11}$$

$$A_y=\frac{2\mathrm{Im}\tilde{t}^{C}(q)\tilde{t}^{LS}(q)^*}{|\tilde{t}^{C}(q)|^2+|\tilde{t}^{LS}(q)|^2} \ , \tag{12}$$

where ρ_J is the isoscalar matter transition density and μ is the reduced projectile energy. Thus, the cross section is proportional to the square of the longitudinal form factor, measured by electron scattering, and to a matter interaction of the form

$$|\bar{t}_m(q)|^2=|\tilde{t}^{C}(q)|^2+|\tilde{t}^{LS}(q)|^2 \ . \tag{13}$$

The relevant components of several effective interactions at zero density are compared in Fig. 3 with the Franey-Love (FL) parametrization of the free t-matrix.[60] The $\mathrm{Re}t_{00}^{C}$ curves seem to be grouped in two pairs. The

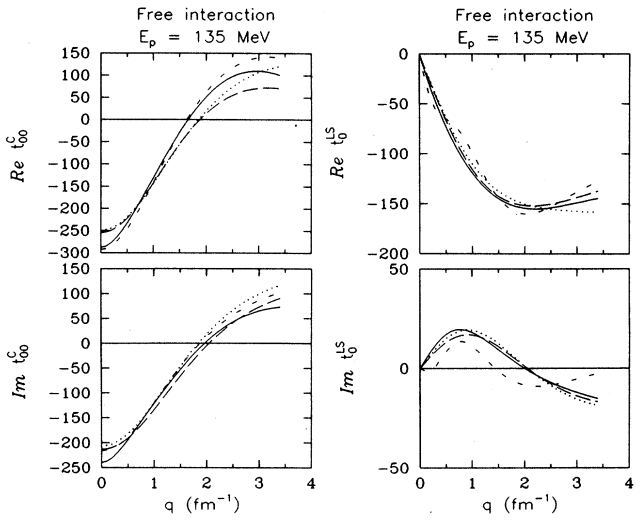

FIG. 3. Free t-matrices for the PH (solid line), BRG (short dashes), NL (dots), and FL (long dashes) interactions. Note that BRG curves were obtained by extrapolation below the smallest tabulated density, $k_F = 0.6$ fm^{-1}.

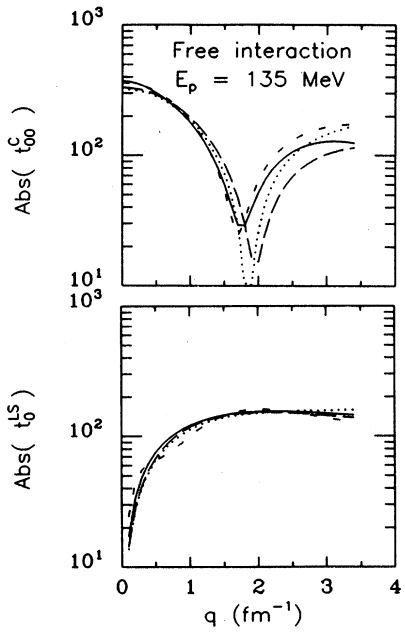

FIG. 4. Moduli of the central and spin-orbit components of the free interaction. The solid curves depict the PH interaction, dots NL, short dashes BRG, and long dashes FL.

Ret_{00}^C components of the PH and BRG interactions are very nearly equal for $q < 2$ fm^{-1}, but then separate at larger momentum transfer. Similarly, the FL and NL interactions produce identical Ret_{00}^C components for $q < 2$ fm^{-1}. However, these two pairs are substantially different from each other. The PH interaction is about 15% stronger than FL at $q = 0$ and has a more rapid q dependence, so that it changes sign first. At $q = 2.5$ fm^{-1}, the Ret_{00}^C component of PH is nearly twice as strong as FL. Although it is not surprising that different t-matrix prescriptions disagree strongly near the maximum momentum transfer available to the two-body system, ambiguities in the off-shell extrapolation may have important implications for the G-matrix that applies to many-body systems.[61]

The Imt_{00}^C components also exhibit a tendency to split into pairs, but these pairs separate at smaller q. Fortunately, the total spread is considerably smaller for Imt_{00}^C than for Ret_0^C. Similarly, the spin-orbit components of the FL, PH, and NL interactions are all quite similar. The BRG spin-orbit components, on the other hand, seem to exhibit rapid oscillations in q. For Ret_0^{LS}, these oscillations are centered upon the average of the other interactions and are probably not too harmful. For Imt_0^{LS}, the BRG interaction is suspect but, fortunately, this component is weak.

The effects these differences among parametrizations of the free t-matrix have on IA predictions are illustrated in Figs. 4 and 5. Figure 4 compares central and spin-orbit moduli and Fig. 5 compares cross sections and analyzing powers. We find that modest variations in $|t_{00}^C|$ for low q become rather strong beyond the node in the central interaction near 2 fm^{-1}. The smaller spread in $|t_0^{LS}|$ tends to dilute this effect upon the matter interaction $|\bar{t}_m|$. The PWIA analyzing power, which changes sign at the node in the central interaction, remains reasonably well defined. Ambiguities in distorted wave impulse approximation (DWIA) calculations due to ambiguities in the t-matrix will be described as bands that represent the spread among calculations using these four representations of the free interaction.

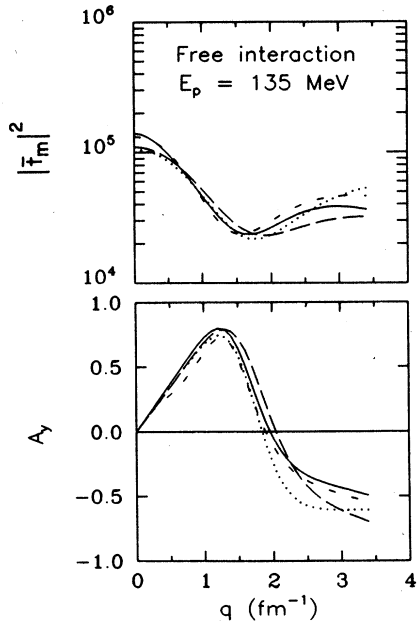

FIG. 5. PWIA matter interaction and analyzing power for normal-parity isoscalar transitions. The various curves display PH (solid line), NL (dots), BRG (short dashes), and FL (long dashes) interactions.

B. Effective interactions for nuclear matter

Several groups have recently addressed the problem of a continuum nucleon in the presence of infinite nuclear matter, all based on the work of Hüfner and Mahaux.[10] Jeukenne, Lejeune, and Mahaux (JLM),[18] who were primarily concerned with properties of the infinite medium, studied the density dependence of the optical potential for nuclear matter. Brieva and Rook[11] then developed a local, density- and energy-dependent effective interaction applicable to the scattering of 0–200 MeV nucleons by finite nuclei. Von Geramb[12–14] has expanded and refined this latter approach and has made available extensive tables of effective interactions based on the Hamada-Johnston[29] (HJ) and Paris potentials.[13] Finally, Nakayama and Love[15] extended the bound G-matrix results of Nakayama *et al.*[62] to the construction of an effective interaction based upon the Bonn potential.

These calculations are all based upon the Bethe-Goldstone equation and include three sources of density dependence. First, Pauli blocking eliminates scattering into occupied intermediate states. Second, the propagator includes a self-consistent optical potential. Third, the effective interaction is reduced to a local form by suitable averaging over relative linear and angular momenta within the Fermi sphere. Mahaux has provided a useful critical review of the nuclear matter theory and its application to finite nuclei in Ref. 63. We contrast the approximations used in the PH and NL calculations in Sec. VI.

Although the general features of the medium modifications are common to all three approaches, the quantitative results depend strongly upon the two-nucleon potential and upon the approximation scheme. The most important medium modifications are found in the isoscalar spin-independent central component of the effective interaction, shown in Fig. 6. The symbols portray the original G-matrix results of Refs. 13, 15, and 29, whereas the curves represent a simpler parametrization to be described below. Density dependence is less important for the spin-orbit interaction because relative s-states are absent. Each interaction is strongly density dependent at 135 MeV. The Pauli inhibition of forward scattering suppresses the effective interaction at small momentum transfer. The anticorrelation between identical nucleons corresponds to an effective short-ranged repulsive interaction which enhances $|\bar{t}_m|^2$ for large momentum transfer. The density dependence is strongest for the BRG interaction, weakest for NL, and intermediate for PH.

The density dependence of the real part of the central interaction is best described by the addition of a short-ranged repulsive core whose amplitude is proportional to density. If this range had been zero, the $\mathrm{Re}\,t_{00}^{C}$ curves plotted in Fig. 6 for several densities would all have been parallel. The range of the repulsive core reduces its effectiveness and causes the curves to draw together for large q.

The density dependence of the absorptive part is best described by a multiplicative damping factor which suppresses the total cross section. According to the estimate of Clementel and Villi (CV),[2] the Pauli blocking factor is approximately

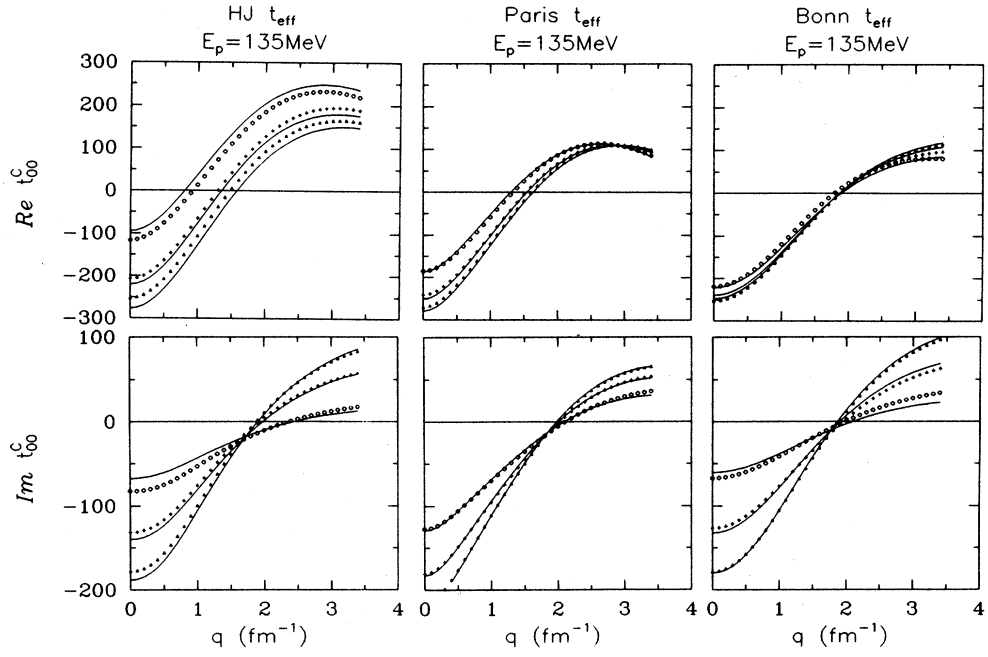

FIG. 6. Central components of the PH, BRG, and NL G-matrices based upon the Paris, Hamada-Johnson, and Bonn potentials. The symbols show original G-matrices for $k_F=0.6$ fm^{-1} (triangles), $k_F=1.0$ fm^{-1} (crosses), and $k_F=1.4$ fm^{-1} (circles). The curves show two-parameter fits.

$$\frac{\bar{\sigma}}{\sigma_0}=1-\frac{7}{5}\frac{\varepsilon_{F_0}}{E_0}\left[\frac{k_F}{k_{F_0}}\right]^2 , \tag{14}$$

where $\varepsilon_{F_0}\simeq 37$ MeV and $k_{F_0}\simeq 1.33$ fm^{-1} represent the Fermi energy and momentum at saturation. Therefore, invoking the optical theorem, we expect Im t to be damped by a factor $(1-a_I\kappa_F^2)$ where $\kappa_F=k_F/k_{F_0}$ and $a_I\approx 0.38$ at $E_0=135$ MeV. More sophisticated nuclear-matter calculations (e.g., Refs. 4 and 11–18) produce damping factors whose form closely resembles the Clementel-Villi (CV) estimate.

These properties of the effective interaction are quite general and can be readily parametrized in the form[38,41]

$$\mathrm{Re}\,\tilde{t}^{\,C}(q,k_F)=\mathrm{Re}\tilde{t}^{\,C}(q,0)+\kappa_F^3\left[a_R+b_R y\left[\frac{q}{\mu_1}\right]\right] , \tag{15a}$$

$$\mathrm{Im}\,\tilde{t}^{\,C}(q,k_F)=[1-a_I\kappa_F^2]\mathrm{Im}\,t^C(q,0)+b_I\kappa_F^2 , \tag{15b}$$

where

$$y(x)=(1+x^2)^{-1}$$

is a Yukawa function and $\kappa_F=k_F/k_{F_0}$. The mass parameter $\mu_1=3.0$ fm^{-1} was chosen somewhat arbitrarily. It is also helpful to represent medium modifications to the real part of the central interaction in the low-q form

$$\mathrm{Re}\tilde{t}^{\,C}(q,k_F)\approx\mathrm{Re}\tilde{t}^{\,C}(q,0)+\kappa_F^3 V_R\left[1-\frac{q^2R^2}{6}\right] , \tag{16}$$

where

$$V_R=a_R+b_R,\quad R^2=\frac{6b_R}{\mu_1^2 V_R} .$$

The parameter V_R measures the strength of the repulsive core and R is range. Similar parametrizations are also available for spin-orbit and tensor interactions.

Although the calculations presented in Secs. IV and V employ the G-matrices in their original forms, the simpler parametrizations given in Eqs. (15) and (16) provide a more useful framework for discussion. The curves shown in Fig. 6 were obtained by reparametrizing the G-matrices. A good description of both the density and momentum-transfer dependence of medium modifications to all three interactions is achieved with only two variable parameters each for the real and for the imaginary parts. The description is best for the PH G-matrix and gives indistinguishable results in scattering calculations. The fit to the BRG effective interaction is not as good. However, this first G-matrix calculation was beset with numerical difficulties that produced somewhat erratic density dependence. A clear illustration of these difficulties may be found in Ref. 64. Hence our smooth parametrization is probably more reliable than the original tables of the BRG interaction. Finally, we notice that the fit to the imaginary part of the NL central interaction is noticeably better than the fit to the real part. The latter could be improved by increasing μ_1 or by altering the exponent of κ_F, but the density dependence of this term is too small to warrant special treatment.

The parameters are collected in Table I. These values were determined for $k_A=2.465$ fm^{-1} and do not include the factor η. For comparison, we have also fitted the JLM interaction assuming $b_R=b_I=0$. We find that the BRG interaction has the strongest repulsive core and the smallest range. The repulsive core of the NL interaction is relatively long ranged but is also rather weak. The real part of the PH interaction is intermediate between these extremes and its density dependence is similar to the JLM result. The damping factors of the PH and JLM interactions are similar to the simple CV estimate, but the damping of the BRG and NL absorptive potentials is considerably stronger. Also note that b_I is small for all three G-matrices.

The effect of density dependence upon cross sections and analyzing powers is illustrated in Fig. 7, where triangles represent one-tenth, crosses one-half, and circles full saturation density. Forward cross sections are suppressed for all three interactions as the density increases. The strong repulsive cores of the PH and BRG interactions enhance the high-q cross section for high densities. Medium modifications to the PH and BRG analyzing powers are similar, but are complicated for low q by competition between effects upon the real and imaginary parts of the central interaction. However, the repulsive core of the NL interaction is too weak to enhance the high-q cross section. Moreover, since most of the NL

TABLE I. Effective interaction parameters.

Source	$\mathrm{Re}t_{00}^{c}(q,0)$ (MeV fm^3)	V_R (MeV fm^3)	R (fm)	$\mathrm{Im}t_{00}^{c}(q,0)$ (MeV fm^3)	a_I [a]	b_I (MeV fm^3)
FL[b]	−255	0.0	0.0	−213	0.0	0.0
JLM[c]	−225	112.0	0.0	−166	0.33	0.0
BRG[d]	−292	169.4	0.78	−215	0.68	−11.8
PH[e]	−287	86.4	1.18	−239	0.44	−5.7
NL[f]	−250	23.8	1.64	−207	0.67	−6.4

[a]For comparison, note that the Clementel and Villi estimate gives $a_I=0.38$ (Ref. 2).
[b]Reference 60.
[c]Reference 18.
[d]Reference 29.
[e]Reference 13.
[f]Reference 15.

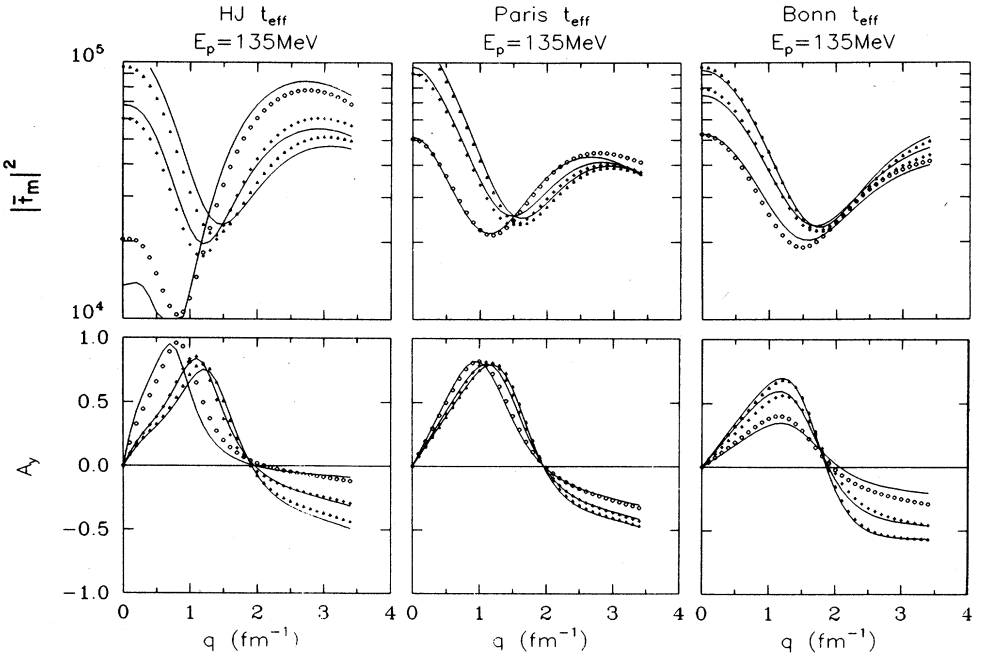

FIG. 7. PWIA matter interactions and analyzing powers for the PH, BRG, and NL G-matrices. The symbols show original G-matrices for $k_F=0.6$ fm^{-1} (triangles), $k_F=1.0$ fm^{-1} (crosses), and $k_F=1.4$ fm^{-1} (circles). The curves result from reparametrization of density dependence.

density dependence resides in $\mathrm{Im}t^C$, we find that the PWIA analyzing power is simply suppressed at high density. Realizing that t^{LS} is predominantly real, the direct correspondence between A_y and $\mathrm{Im}t^C(q,k_F)$ for the NL interaction follows simply from Eq. (12).

Therefore, although the medium modifications predicted by the three available nuclear matter calculations are qualitatively similar in form, the quantitative differences are quite remarkable and will produce distinctive effects upon predicted observables. The range of variation among these G-matrices is much larger than for the corresponding t-matrices. However, it is not yet clear whether the G-matrix amplifies differences between two-nucleon potentials or is vulnerable to uncontrolled approximations. In either case, our parametrization of density dependence can be used to extract parameters from scattering data as a test of improved theories of the effective interaction.

C. Local density approximation

In the folding model, the scattering potential is obtained by convolution of the transition density with the effective interaction. The local-density approximation stipulates that in any small region of a finite nucleus, this effective interaction is the same as that appropriate to infinite nuclear matter whose density is the same as that in the interaction region.

For the strong normal-parity transitions considered in the present work, the transverse form factors have been measured and are small, indicating that the convection and spin densities are negligible. The scattering potential $U(\mathbf{r})$ seen by the incident nucleon then contains only two important terms

$$U(\mathbf{r})=U^C(\mathbf{r})+\nabla U^{LS}(\mathbf{r})\otimes\frac{1}{i}\nabla\cdot\boldsymbol{\sigma} \tag{17}$$

obtained by folding central spin-independent and spin-orbit components of the effective interaction with the transition density. For isoscalar transition densities in a self-conjugate nucleus, charge symmetry ensures that the proton and neutron transition densities are very nearly equal. The point proton density is then obtained by unfolding the proton form factor from the transition charge density. The ground-state density for ^{16}O is taken from Ref. 65 and the transition densities from Ref. 24.

In the pseudopotential approximation, the multipoles of

$$U^C(\mathbf{r})=\sum_J U_J^C(r)\cdot Y_J(\hat{\mathbf{r}})\ , \tag{18a}$$

$$U^{LS}(\mathbf{r})=\sum_J U_J^{LS}(r)\cdot Y_J(\hat{\mathbf{r}})\ , \tag{18a}$$

take the form

$$U_J^C(r)=\frac{2}{\pi}\int dq\, q^2 j_J(qr)\tilde{t}^{\,C}(q)\tilde{\rho}_J(q)\ , \tag{19a}$$

$$U_J^{LS}(r)=\frac{2}{\pi}\int dq\, q^2 j_J(qr)\tilde{\tau}^{\,LS}(q)\tilde{\rho}_J(q)\ . \tag{19b}$$

Density dependence is included most simply by evaluating the interaction

$$\tilde{t}(q)\rightarrow\tilde{t}(q,\rho_g(r)) \tag{20}$$

using the local ground-state density $\rho_g(r)$ at the site of the projectile.

Although the above implementation of the LDA is numerically simplest, it is not unique. The coordinate-space form

$$U^C(\mathbf{r}_1)=\int d^3r_2[t^D(s,\rho_g)\rho(\mathbf{r}_2) + j_0(ks)t^X(s,\rho_g)\rho(\mathbf{r}_1,\mathbf{r}_2)] \tag{21}$$

proposed by Brieva and Rook[11] is more flexible. In this expression, $\mathbf{s}=\mathbf{r}_1-\mathbf{r}_2$ is the separation between a projectile at $\mathbf{r}_1$ and a target nucleon at $\mathbf{r}_2$ and k is the local wave number. The ground-state density ρ_g may be evaluated at r_1, r_2, or their midpoint $c=|\mathbf{r}_1+\mathbf{r}_2|/2$. The spherical Bessel function arises from a short range expansion of the exchange potential. The mixed transition density is assumed to be adequately described by

$$\rho(\mathbf{r}_1,\mathbf{r}_2)=\rho(\mathbf{r}_2)C(k_Fs)\ , \tag{22}$$

where C represents a correlation function.

D. Exchange approximations

In the zero-range exchange approximation (ZREA), we assume that knock-on exchange is dominated by momentum transfers very nearly equal to the incident momentum.[7] The range of the exchange interaction is then so small that the correlation function can be replaced by unity. The pseudopotential approximation is recovered if $j_0(ks)$ is also approximated by unity. The approximation in which $C\rightarrow 1$ but $j_0(ks)$ is retained will be called finite-range exchange (FREA) to distinguish it from the ZREA in which both factors become unity.

In the Slater exchange approximation (SEA), the correlation function for elastic scattering is obtained from the Fermi gas model. For inelastic scattering, an approximate form appropriate for excitations near the Fermi surface is used. These functions are[57]

$$C_{\mathrm{SEA}}(x)=\begin{cases}3\dfrac{j_1(x)}{x} & \text{elastic}\\ j_0(x) & \text{inelastic}\end{cases} \tag{23}$$

and provide the most natural approximation to the nonlocal amplitude.[58] A further refinement of the SEA accounts for the nonuniformity of a finite system by modifying the Fermi momentum appearing in the correlation function.[66,67] These "curvature corrections" turn out to be negligible for the scattering of 135 MeV nucleons.

Another refinement of the exchange approximation is the use of the local energy (LEA)

$$E(r)=E_p-\mathrm{Re}U^C(r) \tag{24}$$

in place of the asymptotic energy (AEA). Although the local energy can affect the direct contribution through the intrinsic energy dependence of the G-matrix, the effect upon the exchange approximation through the wave number is usually more important. However, we find that the largest effect using the 135 MeV PH interaction is a 6% reduction in the central depth of $\mathrm{Re}U^C$ and that LEA and AEA scattering calculations are practically indistinguishable. Hence, we employ the simpler AEA.

E. Effective interaction for inelastic scattering

The hole-line expansion of the effective interaction t' for inelastic scattering contains contributions not present for the elastic interaction. Using the collective model, Cheon *et al.*[39] suggested the relationship

$$t'=\left[1+\rho\frac{\partial}{\partial\rho}\right]t \tag{25}$$

and found that this enhancement of the density dependence improves the agreement between calculations and data for inelastic scattering. Later, Cheon *et al.*[39] showed that the rearrangement factor $(1+\rho\partial/\partial\rho)$ represents a good approximation to the diagrammatic expansion of the inelastic interaction. The relationship also applies to relativistic theories.[40]

The rearrangement factor is particularly easy to apply to parametrizations similar to Eq. (15), for which an elastic medium modification proportional to k_F^n is enhanced for inelastic scattering by a factor of $(1+n/3)$. Thus, medium modifications for inelastic scattering are about twice as strong as those for elastic scattering. We have found that this relationship is crucial to a consistent description of elastic scattering using an empirical effective interaction whose parameters are fitted to data for inelastic scattering.[41–43]

F. Distorted wave approximation

The distorted wave approximation is based upon a Schrödinger equation, modified to include relativistic kinematics, of the form

$$(p^2-k^2+2\mu U)\Psi=0\ , \tag{26}$$

where k is the exact relativistic wave number and μ is the reduced total energy.[68] Consistency between elastic and inelastic scattering requires that distorted waves be generated by the microscopic optical potential corresponding to the same effective interaction that induces the inelastic transition. However, we generally find that there is little qualitative difference between LDA calculations of inelastic cross sections using consistent distorted waves or using a Woods-Saxon optical potential.[19,38,49] The IA is more sensitive to this choice because the absorptive potential predicted by the IA is unrealistically strong. Furthermore, inelastic analyzing power calculations for the LDA are improved by use of consistent optical potentials, largely through the influence of enhanced repulsion upon the real central potential, whereas IA analyzing power calculations are degraded by their own optical potentials.[19]

We do not include Kerman-McManus-Thaler (KMT) factors of $A/(A-1)$.[1] These factors are not applicable to effective interactions for nuclear matter. To maintain consistency between effective interactions at low density

and the t-matrix, KMT factors are not included in IA calculations either. In any case, the effect of such factors upon elastic scattering and upon distorted waves is small for ^{16}O.

IV. ELASTIC SCATTERING

Optical potentials for elastic scattering of 135 MeV protons are compared in Fig. 8 for the FL, BRG, PH, and NL interactions. The LDA was evaluated at the midpoint between projectile and target nucleon positions and exchange was included using ZREA and AEA. Other variations of the LDA and the exchange approximation result in only minor differences. As expected, LDA potentials all approach the IA in the low-density surface region. Central potentials are subject to strong medium modifications, but the effect on the real part of the spin-orbit potential is small. Although the medium modification of the imaginary spin-orbit potential is relatively large, this potential is too small to exert much influence upon the calculations.

Relative to the IA, the LDA imaginary central potentials are smoothly damped in the interior. Although the form of the medium modification is qualitatively the same for all three effective interactions, and in agreement with Eq. (15), the central depths vary by about ±20% among these potentials. The PH potential remains the most absorptive, whereas the NL interaction produces the weakest absorption. These trends are reflected in the a_I parameters listed in Table I.

The LDA real central potentials display more radial structure than the IA or Woods-Saxon potentials. The structure is produced by competition between the attractive and repulsive components of the interaction. For a uniform density, the net potential is attractive. However, the repulsion grows as the density increases. Therefore, the balance between attraction and repulsion is altered in the region of changing nuclear density. The details of the balance depend upon the difference between the gradient of the density and the gradient of the repulsive component. In the energy regime $E_p = 100$–400 MeV, this competition produces a characteristic depression of the real central optical potential inside the nuclear surface.[69] This characteristic radial feature also arises in several other approaches, including Dirac-Hartree calculations,[70] nonstandard phenomenology,[71] and Dirac phenomenology.[72]

The surface depression produced by the BRG interaction (short-dashed curve) is deepest for two reasons. First, among the interactions considered, the low-density limit of the BRG interaction is the strongest at high q. Second, because the density dependence of the real central component of the BRG effective interaction is so strong, as indicated by the V_R parameter Table I, the interaction weakens rapidly across the nuclear surface. On the other hand, the repulsive core for the NL interaction (dotted curve) is relatively weak, and hence the real central potential produced by the NL interaction remains almost as attractive as the IA. Finally, the real central potential produced by the PH interaction (solid curve) is intermediate between these extreme cases.

The impulse approximation for elastic scattering of 135 MeV protons by ^{16}O is compared with the data in Fig. 9. The bands represent the range of variation due to ambiguities in the free t-matrix and show that the essential features are unambiguous. The IA substantially overpredicts the forward cross section and possesses too little structure at larger angles. This lack of structure is related to the insufficient surface stiffness of the IA optical potential, which resembles a Gaussian more than a Woods-Saxon shape. The IA analyzing power is generally positive and fails to describe the deep negative excursions ex-

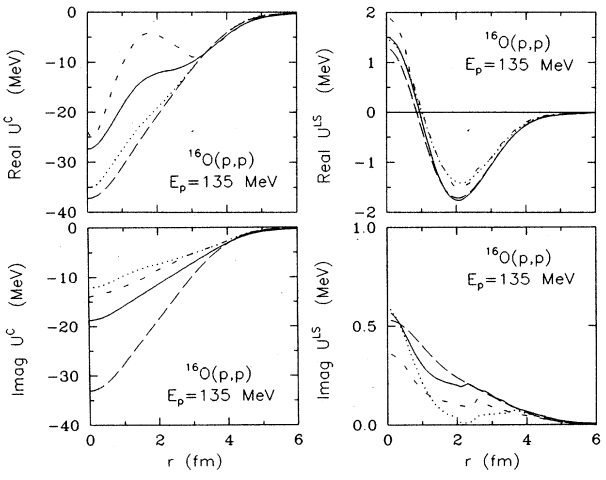

FIG. 8. Optical potentials for scattering of 135 MeV protons by ^{16}O. The solid curves arise from the PH interaction, dots from NL, short dashes from BRG, and long dashes from FL.

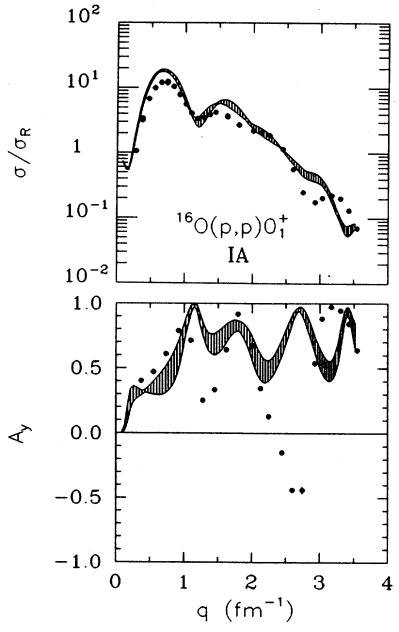

FIG. 9. Impulse approximation for elastic scattering of 135 MeV protons by ^{16}O. The bands span the predictions of four parametrizations of the free interaction and show that problems with the IA are unambiguous. Elastic cross sections are presented as ratios to Rutherford (σ_R) to enhance detail.

hibited by the data.

LDA predictions are shown in Fig. 10 for the BRG, PH, and NL effective interactions. The HJ potential provides a better estimate of the forward cross section, but the high-q structure in the real central potential produces far too much high-q scattering. The softer Paris potential provides a better description of the elastic cross section. In fact, the Paris potential even provides a better description of the elastic scattering data than was possible with a Woods-Saxon phenomenological optical potential. Both the BRG and PH interactions provide much better analyzing power predictions than the IA. However, the A_y oscillations are somewhat too strong with the BRG interaction and somewhat too weak with PH. The NL interaction, on the other hand, fares little better than the IA. Although this effective interaction yields more structure in the cross section, its forward scattering remains too strong presumably because its Re U^C is near the IA. The NL analyzing power prediction is completely out of phase with the data. Therefore, the best description of the elastic scattering data is provided by the PH interaction. It also appears that this description could be improved by slightly stronger density dependence.

Note that none of these potential is strong enough to introduce an additional oscillation in the elastic wave functions within the range of the potential. The change in period is quite small. Therefore, there is no phase-averaging effect involved in comparing inelastic-scattering calculations using distorted waves produced by these various potentials. The primary difference between these sets of distorted waves is their absorption profiles.

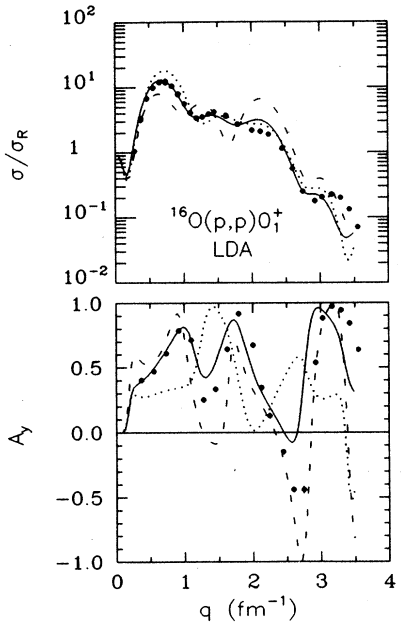

FIG. 10. LDA predictions for elastic scattering based upon the PH (solid line), NL (dots), and BRG (dashes) interactions. The PH interaction gives the best results.

V. INELASTIC SCATTERING

A. IA results

Calculations for two representative states suffice to illustrate the deficiencies of the impulse approximation. We choose the 1_1^- and 3_1^- states of ^{16}O. The surface peaked 3^- state is most sensitive to the low-density properties of the effective interaction, whereas the interior 1^- state samples the interaction near saturation density.

Distorted waves were generated by the PH potential, which gives the best available description of elastic scattering. Note that use of the IA optical potential, although more consistent, would be misleading because the unrealistically strong absorption predicted in the absence of Pauli blocking would strongly suppress inelastic cross sections and also distort the analyzing power. This effect was illustrated in Ref. 38, wherein it was also shown that there is little qualitative difference between inelastic calculations using distorted waves generated by PH or Woods-Saxon potentials.

The bands shown in Fig. 11 reflect the variation in IA predictions based upon the FL interaction and the low-density limits of the three effective interactions. Although analyzing power ambiguities are larger than cross section ambiguities, the essential features of both quantities are unambiguous.

In this model the forward-angle cross sections are dominated, particularly for low multipolarity, by the central interaction. The IA predictions are considerably larger than the cross-section data at forward angles, near the attractive maximum of the central interaction, and then fall well below the cross-section data for larger momentum transfers, near the repulsive maximum of the central interaction. The IA analyzing-power predictions are generally positive, failing to describe the strong nega-

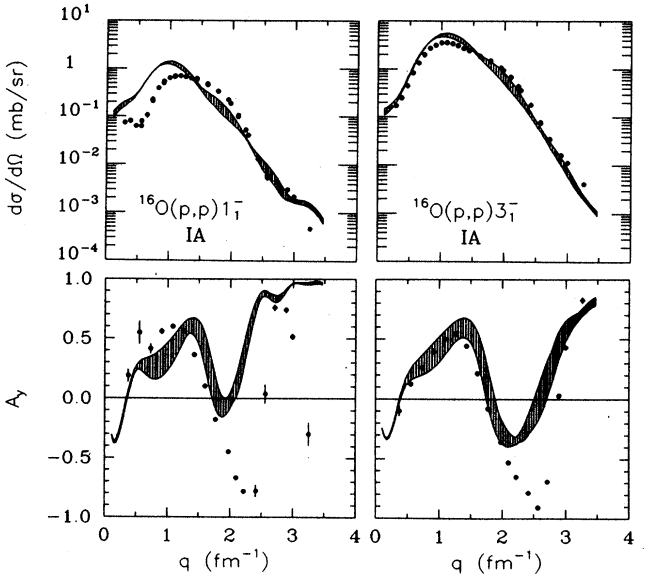

FIG. 11. IA calculations for the 1_1^- and 3_1^- states of ^{16}O. The bands span four interactions and show that there is little ambiguity in the IA.

tive analyzing powers observed for momentum transfer near 2.5 fm^{-1}. The IA also fails to describe the forward analyzing-power minima for 0^+ and 2^+ states.[41–43] This particular failure is also observed in the IA elastic analyzing power.

The failure of the IA is particularly severe for those states whose transition densities are concentrated in the high-density nuclear interior where the medium corrections are expected to be most important.[19] These states include the 1_1^- state and the inelastic monopole states. Moreover, these transition densities have a node near the nuclear surface, resulting in a cancellation between the high- and low-density contributions that is very sensitive to detailed changes in the interaction and the distorted waves. For the 1^- state, the IA overestimates the forward angle cross section by factors of 4–5. As shown in Ref. 41, this factor becomes nearly 10 for monopole states. Moreover, IA analyzing power predictions bear little resemblance to the data. These shortcomings of the IA are common to all strong normal-parity transitions induced by protons near 150 MeV and are not unique to oxygen.[19] Nor are they significantly affected by ambiguities in the free t-matrix, the choice of distorted waves, or exchange approximation. These comparisons clearly show that the effective interaction depends upon density.

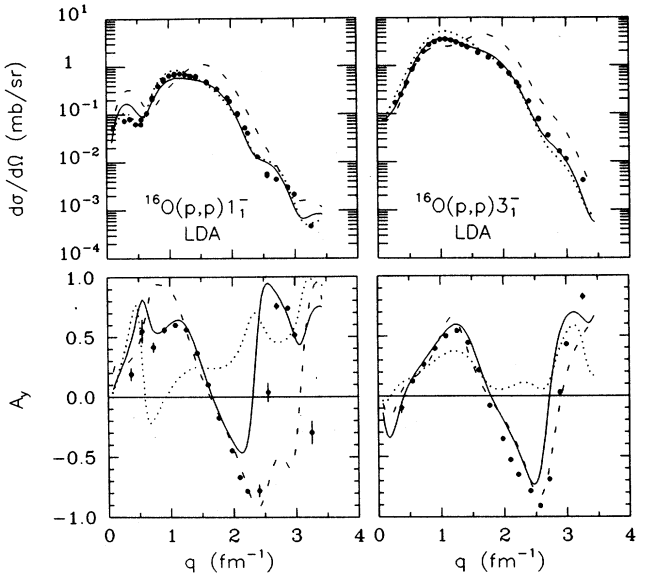

FIG. 12. LDA calculations for the 1_1^- and 3_1^- states of ^{16}O based upon the PH (solid line), NL (dots), and BRG (dashes) interactions. These calculations use consistent distorted waves and include the inelastic rearrangement factor.

B. LDA results

The essential results of this paper are contained in Figs. 12–15, which compare the data with LDA calculations based upon the HJ, Paris, and Bonn potentials. For this set of calculations, the LDA was evaluated at the midpoint between projectile and struck nucleon positions and exchange was included using ZREA and AEA. Consistent distorted waves generated by the microscopic optical potential corresponding to the same effective interaction inducing the inelastic transition were used for each of the three effective interactions under consideration. The $(1+\rho\partial/\partial\rho)$ rearrangement factor was included in the inelastic interaction. Coulomb excitation was also included.

The best overall description of the data is provided by the PH interaction. Forward angle cross sections are reduced by the low-q suppression of the central interaction for high densities. The factor of ten reduction of the low-q 0_3^+ cross section and the factor of four for the 1^- cross section are fully explained by this density dependent interaction. Similarly, the smaller reduction of the low-q cross section for the surface 3^- state is also accounted for. The repulsive maximum of the central contribution to the 1^- cross section near 2 fm^{-1} is significantly enhanced by the medium corrections. This enhancement is required by both the cross-section and analyzing-power data. The negative depths of the analyzing powers for the 1_1^-, 3_1^-, and 4_1^+ transitions are improved by the density-dependent high-q enhancement in the region of the repulsive maximum. Similarly, the negative analyzing powers are deepened for the 0^+ and 2^+ states which have an additional oscillation due to the node in their form factors.

Several systematic trends can be discerned in the remaining deficiencies of the PH interaction. Among this group of states, the 2_1^+ and 4_1^+ transition densities peak at the largest radii, even larger than the 3_1^- density. Yet, we find that the cross sections computed for low-q remain above the data. This observation suggests that the effective interaction is modified even for low densities. Alternatively, multi-step contributions may become visible at this level of precision.[73] We also observe that high-q analyzing powers do not become sufficiently nega-

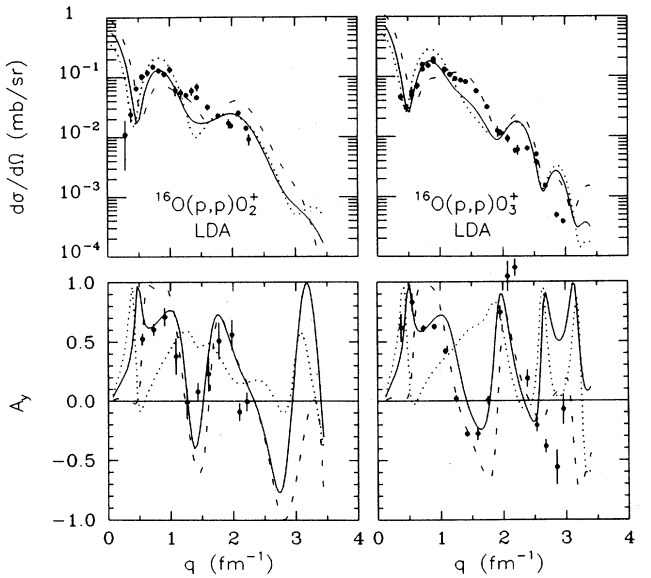

FIG. 13. LDA calculations for the 0_2^+ and 0_3^+ states of ^{16}O based upon the PH (solid line), NL (dots), and BRG (dashes) interactions. These calculations use consistent distorted waves and include the inelastic rearrangement factor.

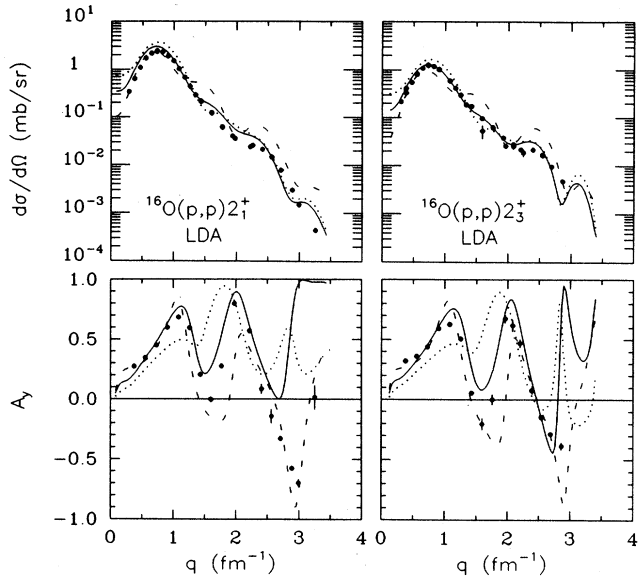

FIG. 14. LDA calculations for the 2_1^+ and 2_3^+ states of ^{16}O based upon the PH (solid line), NL (dots), and BRG (dashes) interactions. These calculations use consistent distorted waves and include the inelastic rearrangement factor.

tive, suggesting that the density-dependent repulsive core of the PH interaction is not quite strong enough.

The dashed curves in Figs. 12–15 show that the density dependence of the BRG interaction is too severe. Cross sections are suppressed too strongly for $0.7 \leq q \leq 1.2$ fm^{-1} and enhanced too strongly for $q > 1.2$ fm^{-1}. [Note that the structure in the 1_1^- cross section for $q \lesssim 0.7$ fm^{-1} is due to distortion.] The structure introduced by medium modifications into the inelastic analyzing power is also too severe with the BRG interaction. Similar defects were also observed for elastic scattering. The conclusion that BRG density dependence is too strong is independent of distorting potential but, as discussed in the following section, is somewhat dependent upon use of the rearrangement factor to enhance inelastic density dependence.

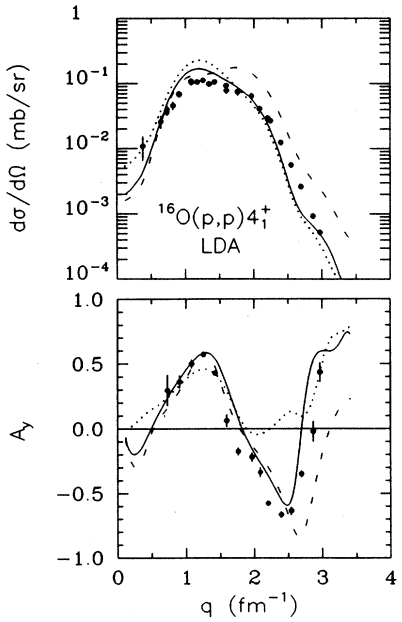

FIG. 15. LDA calculations for the 4_1^+ state of ^{16}O based upon the PH (solid line), NL (dots), and BRG (dashed) interactions. These calculations use consistent distorted waves and include the inelastic rearrangement factor.

The dotted curves in Figs. 12–15 show that the density dependence of the NL interaction is inadequate to describe normal-parity isoscalar transitions. These calculations are not improved by using other optical potentials or reasonable variations of the LDA. Although the cross sections produced by the NL and PH interactions are not very different, the analyzing powers produced by NL are quite poor. The most important differences between these interactions are found in the central components. At zero density, the imaginary part of the NL interaction is stronger at high-q and the real part weaker than corresponding components of the PH interaction. These differences are exacerbated by medium modifications which are stronger in the NL interaction for the imaginary part and weaker for the real part than in the PH interaction. The optical potentials of Fig. 8 illustrate these differences clearly—the real part of the NL potential remains close to the IA but the imaginary part is suppressed substantially more than that of the PH potential.

The problems with the real and imaginary parts of the NL central interaction tend to compensate for each other in cross section calculations but to reinforce each other for analyzing powers. These contrary tendencies are illustrated by Fig. 7 and stem from Eqs. (11) and (12). The cross section depends upon the moduli of the central and spin-orbit interactions, whereas the analyzing power depends upon interference between these contributions. Although the real and imaginary central components of the NL interaction individually differ from corresponding components of the PH interaction, the moduli and cross sections are similar. However, the phases and analyzing powers are rather dissimilar.

These comparisons clearly show that inelastic scattering data are sensitive to details of the effective interaction and its density dependence. Our results support the moderate repulsion and damping features of the PH effective interaction. The density dependence of the BRG interaction, especially the strength of its repulsive core, is too severe. The medium modifications of the NL interaction are too strong for the imaginary central potential and too weak for the real central potential. It appears that the PH description of inelastic scattering could be improved by somewhat stronger damping for low density and somewhat stronger repulsion for high density.

C. Sensitivity to approximations

In this section, we examine the sensitivity of the LDA results to several plausible variations of the reaction model. We begin with the PH interaction, which emerged from the previous section as the most successful predictor of normal-parity isoscalar transitions. Three variations

of the reaction model are compared in Fig. 16. The standard model is represented by the solid curves common to each panel. Interior transition densities yield the greatest sensitivities. Hence, we illustrate these effects for the 1_1^- state of ^{16}O. The sensitivity of elastic scattering calculations and of surface-peaked transitions, such as the 3_1^-, are much smaller and almost indiscernible on similar plots. Sensitivity to the optical potential has been discussed in several previous publications and will not be addressed further.[19,38] Therefore, all calculations in this section use distorted waves emanating from the appropriate optical potentials from Fig. 8.

The leftmost panels of Fig. 16 illustrate the importance of the rearrangement factor. The solid curves represent our standard model, including the $(1+\rho\partial/\partial\rho)$ rearrangement factor due to Cheon.[39,40] The dashed curves illustrate the effect of removing the rearrangement factor. The dotted curves portray IA calculations from which inelastic density dependence is removed altogether. When the inelastic density dependence is enhanced, the description of inelastic scattering becomes comparable in quality to that achieved for elastic scattering. Similar results obtained in Ref. 41 for other states of ^{16}O also support the rearrangement factor. We also note that empirical effective interactions fitted to data for inelastic scattering are not compatible with elastic scattering unless the $(1+\rho\partial/\partial\rho)$ relationship is invoked.[41] Therefore, we conclude that the data support the rearrangement contribution to inelastic potentials proposed by Cheon *et al.*[39,40]

The middle panels of Fig. 16 consider the ambiguity with respect to local density. The similarity between the

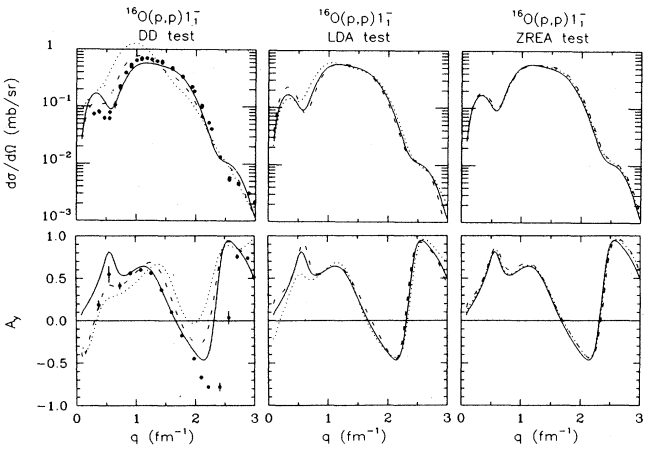

FIG. 16. Variations of the LDA for the 1_1^- state using the PH interaction. The leftmost panels compare the full inelastic density dependence (solid line), the bare elastic G-matrix (dashes), and the density-independent interaction (dots). The middle panels compare local densities evaluated at the projectile position (dots), the struck-nucleon position (dashes), and their midpoint (solid line). The rightmost panels compare ZREA (solid line), FREA (dots), and SEA (dashes) versions of the exchange approximation. Data are omitted from the middle and right panels so that small differences are not obscured. Of these variations, we find that the rearrangement factor is the most important.

surface thickness of nuclei and the range of the effective interaction is cause for concern about the applicability of the local density hypothesis, especially for ^{16}O. The sensitivity of inelastic scattering to ambiguities in the prescription for local density is tested by evaluating the local density at the position of the projectile (dotted curves), or the struck nucleon (dashed curves), or their midpoint (solid curves). Not surprisingly, we find that density dependence is somewhat stronger when evaluated at the struck-nucleon position and somewhat weaker when evaluated at the projectile position than obtained at the average position. However, with the PH interaction we find that the 1_1^- transition is relatively insensitive to these variations and surface-peaked transitions are even less sensitive. We also find that elastic scattering is insensitive to reasonable variations of the local density prescription.

Two factors help limit sensitivity to the LDA prescription. First, because density dependence suppresses the low-q contribution of the central interaction, the relative contribution of the short-ranged spin-orbit interaction is enhanced. The density dependence of this term is relatively small and was evaluated at the projectile position in all cases. Second, the medium modification of the real part of the central interaction is a short-range repulsive core. This contribution is relatively insensitive to ambiguities in the LDA prescription and becomes most important at high momentum transfer.

The rightmost panels of Fig. 16 show that the ZREA, FREA, and SEA versions of the local exchange approximation all give practically identical results for the 1_1^- transition. Similar results are obtained for elastic scattering and for surface excitations. Furthermore, it makes virtually no difference whether the asymptotic or the local wave number is used in the exchange contributions at 135 MeV.

Comparable calculations for the BRG interaction, shown in Fig. 17, are more sensitive to ambiguities in the reaction model because the density dependence is stronger. This increased vulnerability is most evident in the leftmost panels of Fig. 17, which show the effect of the rearrangement factor. In fact, the BRG calculations are improved by omission of rearrangement. The dashed curves of Fig. 17 are similar to the results we obtained[19,38] prior to the publication of Ref. 39 proposing the rearrangement factor. In several of those papers, we concluded that the stronger density dependence of the BRG interaction (without rearrangement) gave a superior description of inelastic scattering but a poor description of elastic scattering, whereas the PH interaction gave good elastic scattering but had inadequate density dependence for inelastic scattering. Consistency is restored when the rearrangement factor bestows adequate density dependence upon the inelastic PH interaction and renders the BRG inelastic interaction as severe as its elastic counterpart.

Calculations using the BRG interaction are more sensitive to the ZREA prescription because the direct and exchange contributions to the central potential are similar in magnitude but opposite in sign; the resultant is only about 20% of either contribution. The BRG exchange

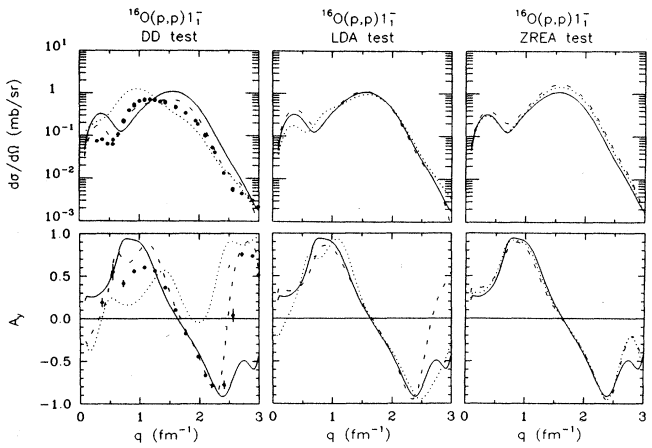

FIG. 17. Variation of the LDA using the BRG interaction. The leftmost panels compare the full inelastic density dependence (solid line), the bare elastic G-matrix (dashes), and the density-independent interaction (dots). The middle panels compare local densities evaluated at the projectile position (dots), the struck-nucleon position (dashes), and their midpoint (solid line). The rightmost panels compare ZREA (solid line), FREA (dots), and SEA (dashes) versions of the exchange approximation.

contribution to the imaginary potential is small. For the PH interaction, on the other hand, the exchange potentials are only about 20% of the direct potentials. The interference is constructive for the real part and destructive for the imaginary part of the central potential. Although the exchange mixture is largely an artifact of the parametrization used to describe the interaction and has little physical significance, it can have important effects upon calculations using approximate treatments of exchange. The PH interaction is superior in this respect.

Finally, we note that even though the BRG calculations are more sensitive to variations of the LDA and ZREA prescriptions, consistent improvement is not obtained for the 1_1^- state, or any of the other states, through these variations. Nor can the NL calculations be salvaged without basic changes in the interaction.

Therefore, we conclude that variations of the effective interaction are much more important than variations of the LDA. The differences seen in Figs. 12–15 among the effective interactions are much greater than the differences seen in Figs. 16–17 for plausible variations of the LDA. This result is important because the LDA has not yet been derived as an approximation for which a systematic series of corrections can be developed and evaluated. Investigations along these lines have been limited to separable potentials and projectile energies below 100 MeV.[74] At present, the LDA must be considered an hypothesis rather than an approximation to an established theory. Fortunately, the ambiguities of the LDA appear sufficiently small to permit clear comparisons to be drawn between the effective interactions that emerge from nuclear matter theory.

D. Special cases

The PH calculations shown in Fig. 18 for the 2_2^+ and 4_2^+ states of ^{16}O are less successful than are the calculations for other states. However, difficulties for these states are not unexpected. The 4_2^+ state lies within 10 keV of an unresolved 3^+ state. Because analyzing powers tend to be small for abnormal-parity transitions, an unresolved abnormal-parity contribution is expected to enhance the cross section and dilute the analyzing power of the doublet. The discrepancies between the PH calculation and the 4_2^+ data are probably due to the unresolved 3^+ state.

The 2_2^+ state, on the other hand, is reached by an abnormally small $C2$ matrix element. Inspection of the γ-decay data compiled within Ref. 75 reveals that the $2_1^+ \rightarrow 2_2^+$ matrix element is about 12 times the direct $0_1^+ \rightarrow 2_2^+$ matrix element. Hence, this transition is a good candidate for two-step excitation through the strong 2_1^+ transition. Such a contribution is expected to enhance the 2_2^+ cross section for momentum transfers in the vicinity of the peak of the 2_1^+ cross section and to dilute the forward-angle analyzing power. The 2_1^+ form factor falls more rapidly with momentum transfer than does the 2_2^+ form factor and should become less influential for high-q. These expectations seem to be supported by the data. However, proof requires a microscopic coupled-channels calculation that is beyond the scope of this paper.

Finally, we observe that a bulge in the 0_3^+ cross section data near 1.5 fm^{-1} is not fully explained by this calculation. However, spin-current effects of the type discussed in Ref. 59 can enhance the 0_3^+ cross section precisely in this region where the electroexcitation form factor passes through a minimum. The effect of the spin-current densi-

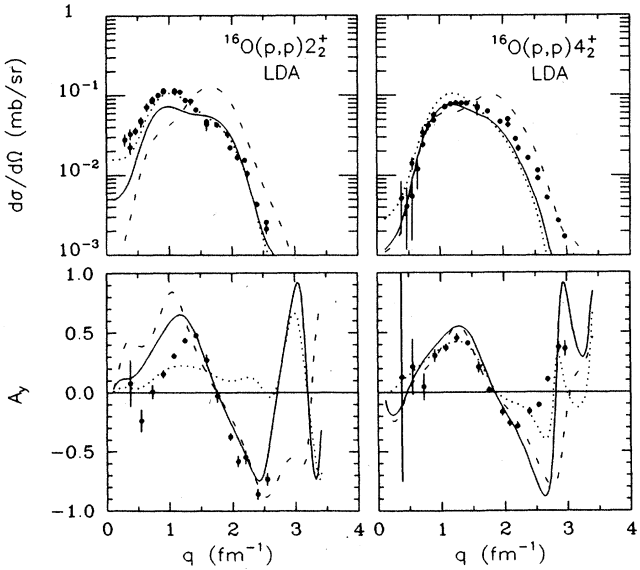

FIG. 18. LDA calculations for the 2_2^+ and 4_2^+ states of ^{16}O based upon the PH (solid line), NL (dots), and BRG (dashes) interactions. These calculations use consistent distorted waves and include the inelastic rearrangement factor.

ty upon the electromagnetic form factor itself is much smaller. Hence, given an accurate reaction model for (p,p'), this interesting transition density could be obtained from a combined fit of the (e,e') and (p,p') data. Again, such an analysis is beyond the scope of this paper.

VI. DISCUSSION

The differences between impulse approximation calculations based upon the free t-matrix and data for inelastic scattering vary in magnitude with the density at which the most important interactions occur. The discrepancies are largest for states with interior transition densities and smallest for states with surface-peaked transition densities. The ability of LDA calculations based upon the PH interaction to provide a uniformly good description of elastic scattering and inelastic scattering for both interior and surface transition densities supports the applicability to finite nuclei of the concept of local nuclear matter density. Calculations of similar quality are also obtained for other nuclei. Therefore, medium modifications to the effective interaction are dominated in the intermediate-energy regime by properties characteristic of the underlying medium. The properties specific to finite systems seem to be less important.

However, it is not yet entirely clear to what extent differences between nucleon-nucleon potentials are more important to the effective interaction than are differences between approximations to the theory of nuclear matter. Each of the three calculations presently available is ostensibly based upon the same theory. For normal-parity isoscalar excitations, each reduces to nearly the same t-matrix for low density. Yet, the medium modifications that emerge from the G-matrix calculations are remarkably different. Although the basic features of damped absorption and enhanced repulsion are common to all three G-matrices, the amplitudes of these features vary widely. Before further insight into the nucleon-nucleon potential can be gleaned from nucleon-nucleus scattering, the theory of effective interactions must be brought under better control. It will be necessary to perform calculations for all three potentials within the same approximation scheme. It will also be necessary to compare each of the approximation schemes for a common potential. Finally, it will be necessary to clearly identify the best approximation scheme and test its convergence.

In the remainder of this section, we contrast the approximations used to reduce the PH and NL calculations to pseudopotential form and attempt to identify the differences which affect the comparisons with experiment. Although the BRG and PH calculations employed different methods to solve the Bethe-Goldstone equation, their constructions of the effective interaction were similar. Hence, we need not consider the BRG calculation further. We focus on the central interaction and use simplified schematic notation.

The G-matrix for nuclear matter is defined by the relationship

$$G\Phi = V\Psi \ , \tag{27}$$

where Φ is the uncorrelated and Ψ the correlated pair wave function. In nuclear matter, these wave functions factor into center-of-mass and relative wave functions according to

$$\Psi = e^{i\mathbf{K}\cdot\mathbf{R}}\psi(\mathbf{r},\mathbf{k},k_F) \ , \tag{28}$$

where

$$\mathbf{k} = \frac{\mathbf{k}_1 - \mathbf{k}_2}{2}, \quad \mathbf{K} = \mathbf{k}_1 + \mathbf{k}_2 \ .$$

The PH calculation is based upon a Bethe-Goldstone equation of the form

$$\psi = \phi + g_Q V \psi \tag{29}$$

where the propagator in nuclear matter is

$$g_Q = \sum_{\substack{k_1' > k_F \\ k_2' > k_F}} \frac{|\mathbf{k}_1'\mathbf{k}_2'\rangle\langle\mathbf{k}_1'\mathbf{k}_2'|}{\varepsilon_1 + \varepsilon_2 - \varepsilon_1' - \varepsilon_2'} \ , \tag{30}$$

and where

$$\varepsilon(k) = \frac{k^2}{2m} + \mathrm{Re}U(k) \tag{31}$$

is the single-particle energy within the self-consistent optical potential U. The NL calculation is based upon the operator equation

$$G = V + Vg_Q G \ . \tag{32}$$

Although Eqs. (29) and (32) are formally equivalent, nonequivalent approximation schemes could produce different G-matrices from the same potential.

Both calculations simplify the Bethe-Goldstone equation by separately averaging the numerator and denominator of g_Q with respect to $\hat{\mathbf{k}}\cdot\hat{\mathbf{K}}$. Similar procedures were used for the numerators, but somewhat different procedures were used for the denominators. The NL calculation used the prescription of Brueckner and Gammel,[76] whereas the PH calculation appears to have used the full angular dependence of the optical potential. However, the PH calculation only iterated U once, starting from zero, while the NL optical potential was fully self-consistent.

The NL calculation used matrix inversion to solve Eq. (32) for matrix elements $G_L(K,k',k,k_F)$ in each partial wave $L \leq 12$. The dependence of G_L upon the momentum of the struck nucleon was eliminated by a very simple averaging procedure. The magnitude of k_2 was chosen as $\frac{3}{4}k_F$, corresponding to a simple average over the Fermi sphere. Then, k and K were determined by unweighted averages over $\hat{\mathbf{k}}_1\cdot\hat{\mathbf{k}}_2$, whereby

$$k = \langle k \rangle = \left\langle \frac{K}{2} \right\rangle = \frac{k_>}{2} + \frac{1}{6}\frac{k_<^2}{k_>} \ , \tag{33}$$

where $k_<$ ($k_>$) is the smaller (larger) of k_1 and $\frac{3}{4}k_F$. This procedure offers the advantage that G reduces to t_{NN} as k_F approaches zero. Moreover, for intermediate energies the conditions $k_1 > 2$ fm^{-1} and $k_2 < 1$ fm^{-1} ensure that $\langle k \rangle$ and $\langle K/2 \rangle$ are within 10% of $k_1/2$ and that k_2 has

little effect upon the density dependence of G. The dependence upon angular momentum was then eliminated by inserting on-shell matrix elements ($k'=k$) into the expansion

$$G(k_1,k_F,q)=\frac{1}{2\pi^2}\sum_L{}'(2L+1)G_L(K,k,k,k_F)P_L(\cos\theta) , \tag{34}$$

where the sum is restricted to partial waves permitted by the Pauli principle. Finally, the fully antisymmetrized matrix elements $G(k_1,k_F,q)$ were expanded in Yukawas according to the pseudopotential prescription of Eqs. (5) and (6) using only on-shell momenta $q<2k$.

A rather more elaborate procedure was used to reduce the PH G-matrix to pseudopotential form. This procedure is based upon the Siemens[77] method and is designed to reproduce, on average, the radial correlations carried by ψ even for small r. For the central interaction, the effective interaction takes the form

$$G(r,k_F,k_1)=\frac{\sum_L{}'(2L+1)\langle j_L(kr)V_L(r)u_L(r,k_F,k,K)\rangle}{\sum_L{}'(2L+1)\langle j_L^2(kr)\rangle} , \tag{35}$$

where the brackets indicate integration over $k_2<k_F$ and where u_L is the correlated radial wave function. Finally, the Fourier transform $G(q,k_f,k_1)$ is fitted by a Yukawa expansion in the range $0\le q\le 5$ fm^{-1}. Such large momenta are required to represent exchange accurately when only the direct potential is fitted.

The most conspicuous advantage of the PH construction is that the off-shell properties of the potential are retained in the small-r behavior of u_L, at least on average. This information is sacrificed by the NL procedure. We speculate that this distinction is the primary reason that the two real central interactions differ so strongly. The short-ranged repulsive core simulates the anticorrelation which tends to keep identical nucleons apart. This effect has important off-shell amplitudes that are retained by the PH construction but discarded by the NL construction. The data clearly show that this short-range repulsion is important. Pauli suppression of the scattering cross section is reflected in on-shell matrix elements and should be adequately described by both procedures.

However, a significant disadvantage of the PH construction is that at zero density the G-matrix is required to reduce to the t-matrix only for $q=0$ and for $q=k_1$. Important differences may appear for intermediate momenta. These discrepancies seem to be especially important for the tensor interaction. Large differences are found between the tensor components of the low-density PH G-matrix and corresponding components of the FL t-matrix. These differences have important implications for the excitation of stretched states. The NL tensor interaction, on the other hand, agrees with the FL t-matrix and gives a better description of data for stretched states than does the PH interaction.[15]

VII. SUMMARY AND CONCLUSIONS

We have measured the differential cross sections and analyzing powers for scattering of 135 MeV protons from ^{16}O for momentum transfers up to 3.2 fm^{-1} and including all narrow states of ^{16}O up to 12.05 MeV excitation. Transition densities deduced from electron scattering measurements were used to minimize structure uncertainties. This analysis has been interpreted as a test of the two-nucleon effective interaction in the nuclear medium, relatively free of nuclear structure uncertainties. An important aspect of this study was the availability of a large range of nuclear transitions with varying radial localization. Interior transitions provide information about the interaction at saturation density, whereas surface transitions are sensitive to the low-density limit of the interaction.

We have identified in the data several striking signatures of density dependence in the isoscalar spin-independent central component of the two-nucleon effective interaction near 135 MeV. As the density increases, the low-momentum-transfer attraction of the effective interaction is suppressed and the high-momentum-transfer repulsion enhanced relative to the free interaction. These medium modifications are manifested by inelastic cross sections that are correspondingly suppressed at low-q and enhanced at high-q relative to impulse-approximation calculations based upon the free interaction and by strong negative analyzing powers near 2.5 fm^{-1} that the IA is unable to reproduce. These signatures are characteristic traits of normal-parity isoscalar excitations of nuclei by 100–200 MeV protons.

The characteristic signatures of density dependence are quite strong and are well described by the local-density approximation based upon effective interactions derived for infinite nuclear matter. The best description of the data for both elastic and inelastic scattering is provided by the effective interaction constructed by von Geramb *et al.*[13,14] from the Paris potential. The inelastic scattering results support the $(1+\rho\partial/\partial\rho)$ relationship between inelastic and elastic interactions that was proposed by Cheon *et al.*[39,40] The results are insensitive to ambiguities in the LDA prescription, exchange approximations, and distorted waves.

However, the results are quite sensitive to the differences between the BRG, PH, and NL effective interactions. Although all of these interactions are based upon essentially the same theory for nuclear matter, the resulting medium modifications differ considerably more than do the free t-matrices for their input potentials. It appears that the approximations made in these three independent calculations are not under good control. To clarify the role played by differences between nucleon-nucleon potentials, it will be necessary to evaluate effective interactions for all three potentials using a consistent approximation scheme and to compare the different approximations made by the three groups with the same potential.

The medium modifications of the effective interaction can be well represented by a very simple parametrization. The imaginary part is subject to a multiplicative damping factor that decreases as the density increases. The

modification of the real part can be represented by an additive short-range repulsive interaction proportional to density. This parametrization can reproduce any of the available theoretical interactions. Alternatively, this parametrization can serve as the basis of a new phenomenology.

Given that the LDA is based upon a truncated nuclear-matter theory whose application to finite systems contains several presently untested assumptions, one does not expect its estimate of the parameters to be completely accurate. Therefore, we propose that these parameters be fitted to a global data set that includes elastic scattering, many inelastic transitions with varying radial localization, and several different target nuclei. It is crucial to this procedure that the target densities be fully constrained by electron scattering. In an extended search procedure, the low-density limit of the interaction might also be optimized. If this program produces a global parametrization that is independent of target and multipolarity and whose parameters vary smoothly with energy, then the LDA description would be considered operationally validated. The remaining task would then be a theoretical explanation of the values of these few parameters. Furthermore, such a parametrization will facilitate the study of structure problems and of neutron densities.[27,78,79]

ACKNOWLEDGMENTS

This work was supported by the National Science Foundation and the U.S. Department of Energy.

---

[a]Present address: IBM Corporation, General Technology Division, Hopewell Junction, NY 12533.
[b]Present address: Department of Physics, College of William and Mary, Williamsburg, VA 23185.
[c]Present address: Department of Physics, University of New Hampshire, Durham, NH 03824.
[d]Present address: Department of Physics, University of Washington, Seattle, WA 98195.
[e]Present address: Los Alamos National Laboratory, Los Alamos, NM 87545.
[f]Present address: Department of Physics, University of Kentucky, Lexington, KY 40506.
[g]Present address: Tektronix Inc., P.O. Box 500, MS 50-271, Beaverton, OR 97077.
[h]Present address: Department of Physics, University of Virginia, Charlottesville, VA 22901.
[i]Present address: Fermilab, Batavia, IL 60510.
[j]Present address: Department of Physics, Bowdoin College, Brunswick, ME 04011.

[1]A. K. Kerman, H. McManus, and R. M. Thaler, Ann. Phys. (N.Y.) **8**, 551 (1959).
[2]E. Clementel and C. Villi, Nuovo Cimento **2**, 176 (1955).
[3]G. L. Shaw, Ann. Phys. (N.Y.) **8**, 509 (1959).
[4]H. R. Kidwai and J. R. Rook, Nucl. Phys. **A169**, 417 (1971).
[5]B. Sinha, Phys. Rep. **20**, 1 (1975).
[6]D. Slanina and H. McManus, Nucl. Phys. **A116**, 271 (1968); D. Slanina, Ph.D. thesis, Michigan State University, 1969.
[7]F. Petrovich, H. McManus, V. A. Madsen, and J. Atkinson, Phys. Rev. Lett. **22**, 895 (1969); F. Petrovich, Ph.D. thesis, Michigan State University, 1971.
[8]G. R. Satchler, Phys. Lett. **35B**, 279 (1971); Comments Nucl. Part. Phys. **5**, 39 (1972).
[9]G. Bertsch, J. Borysowicz, H. McManus, and W. G. Love, Nucl. Phys. **A284**, 399 (1977).
[10]J. Hüfner and C. Mahaux, Ann. Phys. (N.Y.) **73**, 525 (1972).
[11]F. A. Brieva and J. R. Rook, Nucl. Phys. **A291**, 299 (1977); **A291**, 317 (1977); **A297**, 206 (1978); **A307**, 493 (1978).
[12]H. V. von Geramb, F. A. Brieva, and J. R. Rook, in *Microscopic Optical Potentials,* edited by H. V. von Geramb (Springer-Verlag, Berlin, 1979), p. 104.
[13]H. V. von Geramb, in *The Interaction Between Medium Energy Nucleons in Nuclei–1982,* AIP Conf. Proc. No. 97, edited by H. O. Meyer (AIP, New York, 1983), p. 44.
[14]L. Rikus, K. Nakano, and H. V. von Geramb, Nucl. Phys. **A414**, 413 (1984).
[15]K. Nakayama and W. G. Love, Phys. Rev. C **38**, 51 (1988).
[16]N. Yamaguchi, S. Nagata, and T. Matsuda, Prog. Theor. Phys. **70**, 459 (1983).
[17]J. P. Jeukenne, A. Lejeune, and C. Mahaux, Phys. Rev. C **10**, 1391 (1974).
[18]J. P. Jeukenne, A. Lejeune, and C. Mahaux, Phys. Rep. **25**, 83 (1976); Phys. Rev. C **15**, 10 (1977); **16**, 80 (1977).
[19]J. Kelly, W. Bertozzi, T. N. Buti, F. W. Hersman, C. Hyde, M. V. Hynes, B. Norum, F. N. Rad, A. D. Bacher, G. T. Emery, C. C. Foster, W. P. Jones, D. W. Miller, B. L. Berman, W. G. Love, and F. Petrovich, Phys. Rev. Lett. **45**, 2012 (1980).
[20]F. Petrovich and W. G. Love, Nucl. Phys. **A354**, 499c (1981).
[21]F. S. Dietrich, R. W. Finlay, S. Mellema, G. Randers-Pehrson, and F. Petrovich, Phys. Rev. Lett. **51**, 1629 (1983).
[22]S. Mellema, R. W. Finlay, F. S. Dietrich, and F. Petrovich, Phys. Rev. C **28**, 2267 (1983).
[23]F. S. Dietrich and F. Petrovich, in *Neutron-Nucleus Collisions–A Probe of Nuclear Structure,* AIP Conf. Proc. No. 124, edited by J. Rapaport, R. W. Finlay, S. M. Grimes, and F. S. Dietrich (AIP, New York, 1985), p. 90.
[24]T. N. Buti, J. Kelly, W. Bertozzi, J. M. Finn, F. W. Hersman, C. Hyde-Wright, M. V. Hynes, M. A. Kovash, S. Kowalski, R. W. Lourie, B. Murdock, B. E. Norum, B. Pugh, C. P. Sargent, W. Turchinetz, and B. L. Berman, Phys. Rev. C **33**, 755 (1986).
[25]T. deForest and J. D. Walecka, Adv. Phys. **15**, 1 (1966).
[26]J. Heisenberg, Adv. Nucl. Phys. **12**, 61 (1981); J. Heisenberg and H. P. Blok, Annu. Rev. Nucl. Part. Sci. **33**, 569 (1983).
[27]J. A. Carr, F. Petrovich, and J. Kelly, in *Neutron-Nucleus Collisions–A Probe of Nuclear Structure,* AIP Conf. Proc. No. 124, edited by J. Rapaport, R. W. Finlay, S. M. Grimes, and F. S. Dietrich (AIP, New York, 1985), p. 230.
[28]F. Petrovich, J. A. Carr, and H. McManus, Annu. Rev. Nucl. Part. Phys. **36**, 29 (1986).
[29]H. V. von Geramb (unpublished).
[30]T. Hamada and D. Johnston, Nucl. Phys. **34**, 382 (1962).
[31]M. Lacombe, B. Loiseau, J. M. Richard, R. Vinh Mau, J. Cote, P. Pires, and R. de Tourreil, Phys. Rev. C **21**, 861 (1980).
[32]L. Rikus and H. V. von Geramb, Nucl. Phys. **A426**, 496 (1984).
[33]H. V. von Geramb, L. Rikus, and K. Nakano, in *Proceedings*

of the 1983 RCNP International Symposium on Light Ion Reaction Mechanisms, Osaka, Japan, 1983, edited by H. Ogate, T. Kammuri, and I. Katayama (Research Center for Nuclear Physics, Osaka University, Ibaraki, Osaka, Japan, 1983), p. 78.

[34]K. Amos, W. Bauhoff, I. Morrison, S. F. Collins, R. S. Henderson, B. M. Spicer, G. G. Shute, V. C. Officer, D. W. Devins, D. L. Friesel, and W. P. Jones, Nucl. Phys. **A413**, 255 (1984).

[35]M. Hugi, W. Bauhoff, and H. O. Meyer, Phys. Rev. C **28**, 1 (1983).

[36]C. Olmer, A. D. Bacher, G. T. Emery, W. P. Jones, D. W. Miller, H. Nann, P. Schwandt, S. Yen, T. E. Drake, and R. J. Sobie, Phys. Rev. C **29**, 361 (1984).

[37]K. H. Hicks, R. G. Jeppesen, C. C. K. Lin, R. Abegg, K. P. Jackson, O. Häusser, J. Lisantti, C. A. Miller, E. Rost, R. Sawafta, M. C. Vetterli, and S. Yen, Phys. Rev. C **38**, 229 (1988).

[38]J. Kelly, in *The Interaction Between Medium Energy Nucleons in Nuclei–1982,* AIP Conf. Proc. No. 97, edited by H. O. Meyer (AIP, New York, 1983), p. 153.

[39]T. Cheon, K. Takayanagi, and K. Yazaki, Nucl. Phys. **A437**, 301 (1985); **A445**, 227 (1985).

[40]T. Cheon and K. Takayanagi, Nucl. Phys. **A455**, 653 (1986).

[41]J. J. Kelly, in *Relations Between Structure and Reactions in Nuclear Physics,* edited by D. H. Feng, M. Vallieres, and B. H. Wildenthal (World Scientific, Singapore, 1987), p. 222.

[42]J. J. Kelley, in *Advanced Methods in the Evaluation of Nuclear Scattering Data,* Vol. 236 of *Lecture Notes in Physics,* edited by H. J. Krappe and R. Lipperheide (Springer-Verlag, Berlin, 1985), p. 335.

[43]J. J. Kelly, in *Current Problems in Nuclear Physics,* Vol. 1 of *Hellenic Physical Society Conference Series,* edited by T. Paradellis and S. Kossionides (Hellenic Physical Society, Athens, 1986), p. 325.

[44]R. Machleidt, K. Holinde, and Ch. Elster, Phys. Rep. **149**, 1 (1987).

[45]A. Nadasen, Ph.D. thesis, Indiana University, 1977 (available as IUCF Internal Report No. 77-5).

[46]B. E. Norum, M. V. Hynes, H. Miska, W. Bertozzi, J. Kelly, S. Kowalski, F. N. Rad, C. P. Sargent, T. Sasanuma, W. Turchinetz, and B. L. Berman, Phys. Rev. C **25**, 1778 (1982).

[47]D. C. Dodder, G. M. Hale, N. Jarmie, J. H. Jett, P. W. Keaton, Jr., R. A. Nisley, and K. Witt, Phys. Rev. C **15**, 518 (1977), and references therein.

[48]P. Schwandt, H. O. Meyer, W. W. Jacobs, A. D. Bacher, S. E. Vigdor, M. D. Kaitchuck, and T. R. Donoghue, Phys. Rev. C **26**, 55 (1982).

[49]J. Kelly, Ph.D. thesis, Massachusetts Institute of Technology, 1981.

[50]P. R. Bevington, *Data Reduction and Error Analysis for the Physical Sciences* (McGraw-Hill, New York, 1983).

[51]See AIP document no. PAPS PRVCA-39-1222-15 for 15 pages containing a complete tabulation of the data described in this paper. Order by PAPS number and journal reference from American Institute of Physics, Physics Auxiliary Publication Service, 335 E. 45th Street, New York, NY 10017. The price is $1.50 for microfiche or $5.00 for photocopies. Airmail additional. Make checks payable to the American Institute of Physics.

[52]S. S. M. Wong, R. E. Azuma, T. E. Drake, J. D. King, and X. Zhu, Phys. Lett. **149B**, 299 (1984).

[53]W. G. Love, M. A. Franey, and F. Petrovich, in *Spin Excitations in Nuclei,* edited by F. Petrovich *et al.* (Plenum, New York, 1984), p. 205.

[54]J. J. Kelly, Phys. Rev. C **38**, 1490 (1988).

[55]F. Petrovich, R. J. Philpott, A. W. Carpenter, and J. A. Carr, Nucl. Phys. **A425**, 609 (1984).

[56]W. G. Love and M. A. Franey, Phys. Rev. C **24**, 1073 (1981); **27**, 438 (1983).

[57]W. G. Love, Nucl. Phys. **A312**, 160 (1978).

[58]F. Petrovich, J. A. Carr, R. J. Philpott, and A. W. Carpenter, Phys. Lett. **207B**, 1 (1988).

[59]F. Petrovich, J. A. Carr, R. J. Philpott, A. W. Carpenter, and J. Kelly, Phys. Lett. **165B**, 19 (1985).

[60]M. A. Franey and W. G. Love, Phys. Rev. C **31**, 488 (1985).

[61]E. F. Redish and K. Stricker-Bauer, Phys. Rev. C **36**, 513 (1987); **35**, 1183 (1987); M. H. Macfarlane and E. F. Redish, *ibid.* **37**, 2245 (1988).

[62]K. Nakayama, S. Krewald, J. Speth, and W. G. Love, Nucl. Phys. **A431**, 419 (1984).

[63]C. Mahaux, in *The Interaction Between Medium Energy Nucleons in Nuclei–1982,* AIP Conf. Proc. No. 97, edited by H. O. Meyer (AIP, New York, 1983), p. 20.

[64]J. J. Kelly and J. A. Carr, in *Spin Excitations in Nuclei,* edited by F. Petrovich *et al.* (Plenum, New York, 1984), p. 253.

[65]H. de Vries, C. W. de Jager, and C. de Vries, At. Data Nucl. Data Tables **36**, 495 (1987).

[66]J. W. Negele and D. Vautherin, Phys. Rev. C **5**, 1472 (1972).

[67]X. Campi and A. Bouyssy, Phys. Lett. **73B**, 263 (1978).

[68]L. Ray and W. R. Coker, Phys. Rev. C **16**, 340 (1977).

[69]P. Schwandt, in *The Interaction Between Medium Energy Nucleons in Nuclei–1982,* AIP Conf. Proc. No. 97, edited by H. O. Meyer (AIP, New York, 1983), p. 89.

[70]M. Jaminon, C. Mahaux, and P. Rochus, Phys. Rev. Lett. **43**, 1097 (1979).

[71]H. O. Meyer, P. Schwandt, G. L. Moake, and P. P. Singh, Phys. Rev. C **23**, 616 (1981); C. W. Glover, P. Schwandt, H. O. Meyer, W. W. Jacobs, J. R. Hall, M. D. Kaitchuck, and R. P. DeVito, *ibid.* **31**, 1 (1985).

[72]B. C. Clark, S. Hama, S. G. Kälbermann, E. D. Cooper, and R. L. Mercer, Phys. Rev. C **31**, 694 (1985); B. C. Clark, S. Hama, and R. L. Mercer, in *The Interaction Between Medium Energy Nucleons in Nuclei–1982,* AIP Conf. Proc. No. 97, edited by H. O. Meyer (AIP, New York, 1983), p. 260.

[73]R. A. Miskimen, A. M. Bernstein, G. Bernhardt, C. F. Williamson, B. A. Brown, and R. Alarcon, Phys. Rev. C **37**, 1600 (1988).

[74]R. Brugger and M. K. Weigel, Phys. Rev. C **35**, 2049 (1987); **37**, 411 (1988).

[75]F. Ajzenberg-Selove, Nucl. Phys. **A375**, 1 (1982).

[76]K. A. Brueckner and J. L. Gammel, Phys. Rev. **109**, 1023 (1958).

[77]P. J. Siemens, Nucl. Phys. **A141**, 225 (1970).

[78]J. J. Kelly, W. Bertozzi, T. N. Buti, J. M. Finn, F. W. Hersman, M. V. Hynes, C. Hyde-Wright, B. E. Norum, A. D. Bacher, G. T. Emery, C. C. Foster, W. P. Jones, D. W. Miller, B. L. Berman, J. A. Carr, and F. Petrovich, Phys. Lett. **169B**, 157 (1986).

[79]J. J. Kelly, Phys. Rev. C **37**, 520 (1988).